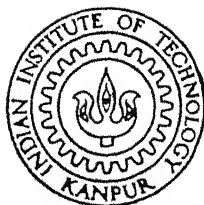


A TWO DIMENSIONAL SIMULATION OF MOSFETS

by
TAPAS NANDI



DEPARTMENT OF ELECTRICAL ENGINEERING
INDIAN INSTITUTE OF TECHNOLOGY KANPUR
MARCH, 1990

EE

1990

M

NAN

TWO

A TWO DIMENSIONAL SIMULATION OF MOSFETS

A Thesis Submitted
in Partial Fulfilment of the Requirements
for the Degree of
M.Tech.

by
TAPAS NANDI

to the
DEPARTMENT OF ELECTRICAL ENGINEERING
INDIAN INSTITUTE OF TECHNOLOGY
KANPUR

March, 1990

EE- 1990-M-NAN-TWO

24 JAN 1991

CENTRAL LIBRARY
1000 1000

109954

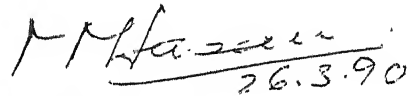
TX

621.3915

N153

CERTIFICATE

This is to certify that this thesis titled "A TWO DIMENSIONAL SIMULATION OF MOSFETS" is a report of work carried out under my supervision by Tapas Nandi and that it has not been submitted elsewhere for a degree.



Handwritten signature of M. M. Hasan, dated 26.3.90.

(M. M. Hasan)

Professor

Department of Electrical Engineering

Indian Institute of Technology

Kanpur - 208016.

ACKNOWLEDGEMENT

I express my deepest gratitude to prof. M.M. Hasan for suggesting the problem, inspiring guidance and invaluable discussions, I had with him during the course of this study.

I am also thankful to Dr. S. Jain, for his excellent suggestions regarding the problems I faced during the initial stage of this thesis work. My sincere thanks go to all the staffs of the computer centre and the library for their prompt co-operation.

This thesis would not have been possible without the help of my friends who have helped me a lot in preparing, proof-reading and printing of this thesis report. I acknowledge their help with gratitude. I, hereby, convey my thanks to all of them who have made my stay at I.I.T., Kanpur, a memorable one.

ABSTRACT

The most effective way to design VLSI MOSFET structures is to use a sophisticated complex two dimensional model. Such a model, using the basic semiconductor equations along with the accurate models for the physical parameters of the basic equations, has been described here. Numerical simulation of this MOSFET model using finite difference method has also been described. Low computation cost algorithms have been used to develop an easy-to-use software package for planar MOSFET simulation. Simulated results are presented for few types of short channel MOSFETs to show the power of the device simulation to predict the behaviour of the device. Finally, the modifications of this MOSFET simulation model and the possibility to integrate this device simulation with the process and the circuit simulations have been proposed.

CONTENTS

Chapter 1	INTRODUCTION	1
Chapter 2	MATHEMATICAL FORMULATION	4
	2.1 Basic equations	4
	2.2 Normalization	6
	2.3 Choice of dependent variables	8
	2.4 Boundary conditions	10
Chapter 3	MODELS & ASSUMPTIONS	15
	3.1 Numerical model for MOSFET	15
	3.2 Other assumptions generally used with level 2 model	17
	3.3 Modelling of the physical parameters	18
Chapter 4	NUMERICAL TREATMENT	27
	4.1 Basic concepts	27
	4.2 Grid formation	28
	4.3 Discretization	30
	4.4 Computer implementation of Bernoulli function	46
	4.5 Adaptive grid generation	48
Chapter 5	ALGORITHMS TO EXTRACT RESULTS	51
	5.1 Gummel's algorithm	51

	5.2	Solution of large sparse linear systems	56
	5.3	Post-processing of ψ , n , p	62
	5.4	Convergence criterion of Gummel's algorithm used	66
Chapter 6		SIMULATED EXAMPLES	68
	6.1	Simulated devices	68
	6.2	Comparison of terminal characteristics of the three devices described	81
	6.3	Simulation of a depletion n-MOSFET	91
Chapter 7		CONCLUSION	93
	7.1	Proposal for further work	93
		REFERENCES	97
		APPENDIX	102

Chapter 1

INTRODUCTION

The development of new semiconductor technologies and novel semiconductor device structures have traditionally been guided by an experimental approach . Starting from an established process sequence , fabrication steps are changed together with geometrical dimensions (feature size). The modified process is then realized by fabricating several lots . The finished devices are tested to insure their performance conforms to the initial design . This approach usually includes several iterations of the process to testing loop . With the advent of increasingly complex integrated circuits , the traditional empirical approach becomes expensive and time consuming .

There are analytical models for the device and the process steps available as an alternative approach towards the design and development of integrated circuits . But all of them use certain assumptions and regional approximations , which are often so restrictive that the predictability of the performance of the devices in the VLSI complexity has turned out to be insufficient.

In order to characterize the modern devices in a reasonable way , higher order *numerical models* emerge out to be the only solution . The extraction of the solution of these numerical models , which approximate the actual physics going on in the devices , in a fabrication process step or in the fabricated

circuit closely, is popularly called as *simulation* . When simulation is done for a device , it is called *device simulation* ; similarly for the fabrication process and for the circuit performance are called *process and circuit simulations* respectively .

The device simulation when coupled with the process simulation and circuit simulation , makes design and development process of VLSI circuits very cost and time effective compared to the experimental approach described before . Basically , the simulation softwares are guided by the principles of robustness , speed of solution , low computation cost and easy user access .

This thesis work deals with the development of a device simulation software and the planar *Metal Oxide Field Effect Transistor* (MOSFET) has been chosen as the device for simulation, because it is the semiconductor device widely used in the VLSI circuits .

The *device simulation* basically means the solution of three coupled non-linear partial differential equations, i.e. Poisson's equation and two current continuity equations , inside the domain of the device (here MOSFET) with proper boundary conditions and with proper models of the physical parameters appeared in the equations mentioned . Basic partial differential equations (called the basic semiconductor equations) which describe the behaviour of the device and their boundary conditions are dealt in *chapter 2* . This chapter also deals with the scaling of these equations for better numerical stability and accuracy .

Chapter 3 contains the models for the physical parameters like carrier mobilities, doping profile etc, and the assumptions imposed on the numerical model of MOSFET to make the computer solution faster without major loss of accuracy .

Numerical methodologies to solve the basic coupled semiconductor equations (i.e., discretization and mesh generation) are given in *chapter 4* . The algorithm for fast and low cost solution methods and post-processing of the results are dealt in *chapter 5*.

Few example devices simulated by the device simulation software developed in this thesis work are described in the 6th *chapter* .

The concluding chapter (*chapter 7*) outlines the scope of the extension and the modification of the simulation software . An *appendix* is also included to explain how to use this device simulation software .

Chapter 2

MATHEMATICAL FORMULATION

2.1. Basic Equations :-

In order to accurately analyze any semiconductor structure, taking all the effects (non-ideal) into account, the basic semiconductor equations must be solved. The following are the equations governing inside semiconductor :

2.1a. Poisson's equation :

$$\nabla^2 \psi = - \frac{q}{\epsilon} (p - n + N_d - N_a) \quad (2.1)$$

where, ψ : electrostatic potential

p, n : hole, electron concentrations

$N_d^+ - N_a^-$: total ionized impurity

ϵ : permittivity of semiconductor

2.1b. Continuity equations :

$$\frac{1}{q} \nabla \cdot J_n = \frac{\partial n}{\partial t} + R \quad (2.2)$$

$$\frac{1}{q} \nabla \cdot J_p = -\frac{\partial p}{\partial t} - R \quad (2.3)$$

where, J_n, J_p : electron, hole current density

R : recombination rate

q : electronic charge

2.1c. Current relations :

$$J_n = -q (\mu_n n \nabla \psi - D_n \nabla n) \quad (2.4)$$

$$J_p = -q (\mu_p p \nabla \psi + D_p \nabla p) \quad (2.5)$$

where, μ_n, μ_p : electron, hole mobilities

D_n, D_p : electron, hole diffusion coefficients

: both of them are functions of electric field, dopant & carrier concentrations.

Under non-degenerate condition $D_{p,n}$ & $\mu_{p,n}$ are related by Einstein relation :

$$D_p = \mu_p kT/q \quad \& \quad D_n = \mu_n kT/q \quad (2.6)$$

where, k : Boltzmann's constant & T : absolute temperature

Under non-degenerate condition n & p are related to ψ by :

$$n = n_i e^{q(\psi - \phi_n)/kT} \quad \& \quad p = n_i e^{q(\phi_p - \psi)/kT} \quad (2.7)$$

where, ϕ_n, ϕ_p : quasi fermi potentials for electron & hole, under equilibrium condition $\phi_n = \phi_p$ & $np = n_i^2$. Where n_i is intrinsic carrier concentration.

Now returning to (2.4) & (2.5) first parts of r.h.s. are drift and second parts are diffusion components of currents. Combining these two parts (i.e., operating ∇ over n & p and using (2.6) & (2.7)) we get,

$$J_n = q \{ D_n n_i e^{\psi/V_T} \nabla (e^{-\phi_n/V_T}) \} \quad (2.8)$$

$$J_p = -q \{ D_p n_i e^{-\psi/V_T} \nabla (e^{\phi_p/V_T}) \} \quad (2.9)$$

where, $V_T = kT/q$: thermal voltage

Now combining (2.8), (2.9), (2.2) & (2.3) to get combined equation for steady state [i.e., $\partial/\partial t \equiv 0$]

$$\nabla \cdot \{ D_n n_i e^{\psi/V_T} \nabla (e^{-\phi_n/V_T}) \} = R \quad (2.10)$$

$$\nabla \cdot \{ D_p n_i e^{-\psi/V_T} \nabla (e^{\phi_p/V_T}) \} = R \quad (2.11)$$

These (2.1), (2.10), (2.11) are the basic equations for the numerical model of semiconductor devices.

2.2. NORMALIZATION :-

In order to get accurate computer solution, we need to scale the basic equations in such a way, that the dependent variables and independent variables vary within allowable limits and become dimensionless. One such normalization scheme is proposed by De Mari [2] is adopted and the scaling factors are tabulated in the table-2.1.

Quantity	Symbol	Expression	Value (At 300°K)
x, y, z	x_0	$L_d = \sqrt{\frac{\epsilon kT}{q^2 n_i}}$	$3.357 \times 10^{-3} \text{ cm}$
ψ	ψ_0	kT/q	0.0259 V
n, p, N_d, N_a	C_0	n_i	$1.5 \times 10^{10} / \text{cc}$
D_n, D_p	D_0	-	$1 \text{ cm}^2 / \text{sec}$
μ_n, μ_p	μ_0	D_0 / ψ_0	$38.61 \text{ cm}^2 / \text{v-sec}$
R	R_0	$D_0 C_0 / x_0^2$	$1.33 \times 10^{15} / \text{cc-sec}$
J_n, J_p	J_0	$\psi_0 n_i kT / x_0$	$7.15 \times 10^{-7} \text{ A/cm}^2$
t	t_0	x_0^2 / D_0	$1.127 \times 10^{-5} \text{ sec}$

Table 2.1
Scaling factors

Normalizing with the scaling factors (2.1), (2.10) & (2.11) become :

$$\nabla^2 \psi = (n - p - C) \quad (2.12)$$

$$\text{where, } -C = N_a^- - N_d^+, \quad n = e^{(\psi - \phi_n)} \quad \& \quad p = e^{(\phi_p - \psi)}$$

$$\nabla \cdot (\gamma_n e^{\psi} \nabla (e^{-\phi_n})) = R \quad (2.13)$$

$$\nabla \cdot (\gamma_p e^{-\psi} \nabla (e^{\phi_p})) = R \quad (2.14)$$

where, γ_n, γ_p : normalized mobilities of electron & hole

All the variables and operators of the main equations written from (2.12) and onwards are normalized. Separate notations are not used for the normalized quantities to distinguish them from the unscaled equations, for convenience of writing.

2.3. CHOICE OF DEPENDENT VARIABLES :-

For analytical purpose it is often helpful to use dependent variables other than n, p in the basic equations (2.12) through (2.14). One set, very frequently used, is $\{\psi, u, v\}$ [Slotboom[5], Adachi et al[11], Hiemier[12] & others]; which relates to the original set $\{\psi, n, p\}$ by :

$$n = e^{\psi} \cdot u \quad \& \quad u = e^{-\phi_n}$$

$$p = e^{-\psi} \cdot v \quad \& \quad v = e^{\phi} p$$

The major advantage is, it makes the continuity equations linear self-adjoint elliptic partial differential equations (P.D.E.). Rugged solution methods are available for this type of problem. It is not used here as the major drawback of these variables is that, u and v need enormous dynamic range of numbers to represent them on computer [u (v) varies more than 33 orders of magnitude for ϕ_n (ϕ_p) variation in -1 to +1 range]. So this set is limited to low voltage applications to semiconductor devices.

Another set of dependent variables is $\{\psi, \phi_n, \phi_p\}$, used as natural consequence from (2.12) through (2.14). An advantage here is that all the dependent variables are of same order of magnitude. Still there is a major disadvantage, all the equations become non-linear. This set has been used by Gummel[1], Meinerzhagen et al [16] and others[19].

The most suitable set is $\{\psi, n, p\}$. The advantages are same as the set $\{\psi, u, v\}$; only poisson's equation is *non-linear elliptic* P.D.E., and continuity equations are *linear self adjoint elliptic* P.D.E.. Moreover the dynamic range for n and p is smaller [varies 16 orders of magnitude at the maximum] than the set of u and v . Fitchner, Rose & Bank [8] pointed out the chance of getting inadmissible and unphysical negative carrier concentrations as the solution of basic equations due to discretization error in difference scheme [discussed later]. But the proper grid structure and proper discretization scheme for continuity equation eliminate

this discrepancy totally. This set was used by Van Dorpe[4], De Mari[2], Selberherr et al[13]. We have chosen this set of dependent variables $\{\psi, n, p\}$.

Mock[6], Toyabe[14], Yamaguchi[20] and others used stream functions as dependent variables in continuity equations. But in this formulation there is no provision for inclusion of recombination-generation term.

2.4. BOUNDARY CONDITIONS :-

Before imposing boundary conditions, we need to discuss the structure of the device and the coordinate system used. Referring to figure(2.1) 'x' is away from Si-SiO₂ interface, and 'y' is from source to drain contact. Since there is no change in n, p & ψ in the bulk of semiconductor when MOSFET operates in subthreshold, linear and active mode computer simulation is done upto a reasonable depth (10 to 20 times the depletion width).

The boundaries present in the MOSFET structure [fig.(2.1)] can be divided into two parts :

2.4a. Real boundaries :

In fig(2.1) ab, ij, bc, cd & kl fall under this category. Now the boundary condition for dependent variables are set as follows:

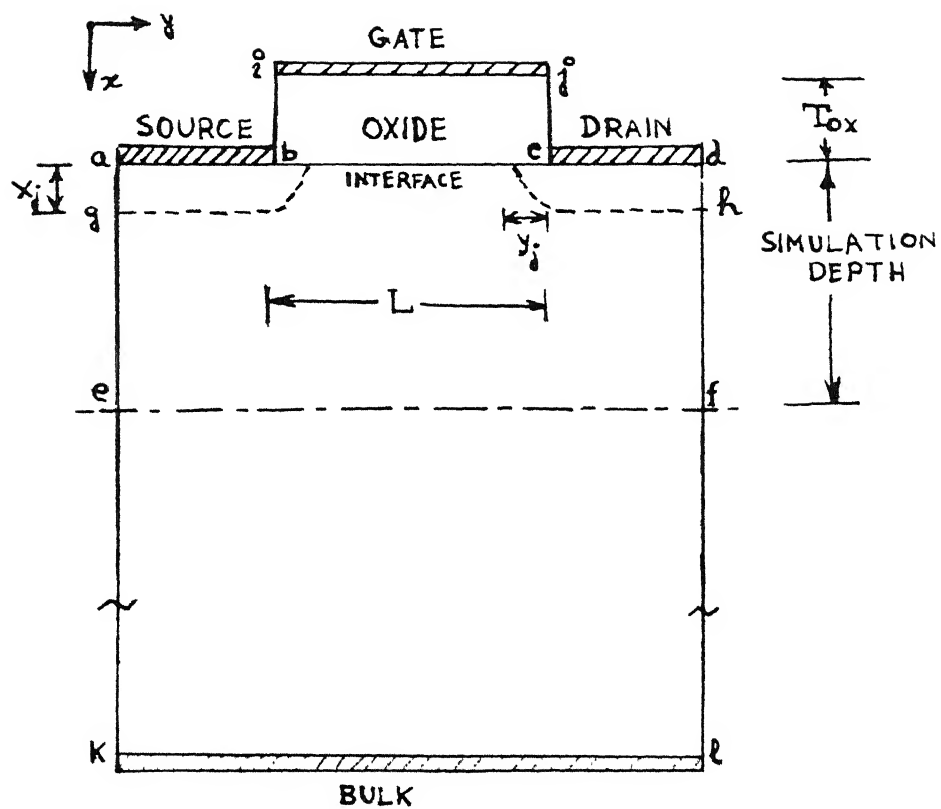


Fig. 2.1
The basic simulation geometry of MOSFET

(i) *Potential* :- At ohmic contacts [ab:source, i]:gate, cd:drain, kl:body] we know the applied potentials. So the value of ψ at these places (Dirichlet boundary), are given by,

$$\psi = V_{\text{applied}} + V_{bi} \quad (2.15)$$

Where, V_{bi} : built-in junction potential (applied bulk voltage is taken as reference, so V_{bi} is added with source and drain voltages).

At Si-SiO₂ interface (bc) Gauss's law is applicable,

$$\epsilon_{si} \left(-\frac{\partial \psi}{\partial x} \right) = \epsilon_{ox} \left(-\frac{\partial \psi}{\partial x} \right) + Q_{int} \quad (2.16)$$

where, Q_{int} : interface trapped charge assumed to be present at the interface as delta function.

ϵ_{si} & ϵ_{ox} : are permittivities of Silicon and Silicon-di-Oxide

$-\frac{\partial \psi}{\partial x}$: is electric field

(ii) *Electron & Hole* :- As proposed by H. K. Gummel[1], we took neutral space charge density and thermal equilibrium for carriers at ohmic contacts, i.e.,

$$n - p - C = 0 ; \quad C = N_d^+ - N_a^- \quad \& \quad n.p = 1$$

Solving these equations :

$$n = \sqrt{\left[(C/2)^2 + 1 \right]} + (C/2)$$

$$p = \sqrt{\left[(C/2)^2 + 1 \right]} - (C/2)$$
(2.17)

It is also clear from $np = 1$ that, ϕ_n, ϕ_p are same at the ohmic contacts.

At the interface, there is no component of current density normal to the boundary (bc) i.e.,

$$J_{nx} = 0 \quad \& \quad J_{px} = 0$$
(2.18)

Corresponding boundary conditions for n & p are derived from (2.18) during discretization of continuity equations.

2.4b. Fictitious boundaries :

They are not the physical limits of the device, but imposed as the boundary of simulation area [aek, dfl, lb, lc, ef of fig.(2.1)].

At these boundaries no changed in dependent variables assumed, i.e., no electric field and no current flowing out of these boundaries.

$$\frac{\partial \psi}{\partial y} = 0, \quad \frac{\partial p}{\partial y} = 0, \quad \frac{\partial n}{\partial y} = 0 \quad (2.19)$$

At the vertical fictitious boundaries.

$$\frac{\partial \psi}{\partial x} = 0, \quad \frac{\partial p}{\partial x} = 0, \quad \frac{\partial n}{\partial x} = 0 \quad (2.20)$$

At the horizontal fictitious boundaries.

Now, with these scaled basic equations and boundary conditions in one hand, we are going to establish the practical numerical model for the MOSFET and other physical parameters like, mobility, doping profile, intrinsic carrier concentration etc. in the next chapter.

Chapter 3

MODELS & ASSUMPTIONS

This chapter consists of the suitable numerical models for the MOSFET and the physical parameters, i.e., carrier mobilities, intrinsic carrier concentration, doping profile of the device under consideration etc.

3.1 . NUMERICAL MODEL FOR MOSFET :-

The model hierarchy consists of three different steady state MOS models . The highest level (level 3) of hierarchy requires numerical solution of two dimensional Poisson's equation and both of the continuity equations in two dimension with appropriate boundary conditions and physical models . Only level 3 model can handle avalanche generation and breakdown in MOSFET. When avalanche generation starts, the coupling between Poisson's and continuity equations becomes very strong; so all the basic equations are to be solved simultaneously (Meinerzhagen et al [16]). This simultaneous solution is very expensive in terms of computer memory and C.P.U time. The two lower level models are valid when there is no generation-recombination.

Level 2 model assumes that there is no minority carrier current [This assumption is supported Selberherr et al :MINIMOS1 [13], Toyabe et al, CADDET [17], De la Moneda [19] and others].

For n-channel MOSFET assumption is :

$$J_p = 0 \quad \text{in the entire device.}$$

So, level 2 model simplifies down to solution of 2-d Poisson's and 2-d majority carrier (electron for n-channel) continuity equation .

Level 1 is the simplest model, assumes no minority carrier current and majority carrier current flows only in lateral (along source to drain) direction . So :

$$\frac{\partial \phi_n}{\partial x} = 0 \quad \text{in the channel region.}$$

With this simplification, solution work tackles only 2-d Poisson's equation and 1-d majority carrier continuity equation. This is quite accurate model in subthreshold and linear regions of MOS I-V characteristics.

We have used, *level 2 model*, as our main interest is to simulate MOS in *subthreshold, linear and active zone* . Moreover level 2 model is quite *economic* in terms of *computer memory and C.P.U. time* . This model is claimed to be reasonably close with the experimental results by several authors [13], [14], [19], [20].

The level 2 model used in this simulation is written again:

(a) N-channel MOS :-

$$\nabla^2 \psi = (n - p - C) \quad (3.1a)$$

$$\nabla \cdot J_n = 0 \quad (3.1b)$$

$$J_p = 0 \quad (3.1c)$$

$$\text{i.e., } \phi_p = \text{constant} \quad (3.1d)$$

(b) P-channel MOS :-

$$\nabla^2 \psi = (n - p - C) \quad (3.2a)$$

$$\nabla \cdot J_p = 0 \quad (3.2b)$$

$$J_n = 0 \quad (3.2c)$$

$$\text{i.e., } \phi_n = \text{constant} \quad (3.2d)$$

3.2. OTHER ASSUMPTIONS GENERALLY USED WITH LEVEL 2 MODEL :-

(i) Homogeneity of permittivity :

$$\epsilon_{\text{si}} = \text{constant}, \epsilon_{\text{SiO}_2} = \text{constant} \quad (3.3a)$$

(ii) Total ionization of all the impurities :

$$C = N_d - N_a = N_d^+ - N_a^- \quad (3.3b)$$

(iii) No band gap narrowing :

Since doping crosses 10^{19} /cc only at positions very close to the ion implanted source and drain contacts, other parts have much less than 10^{19} /cc impurity concentration. So we assume,

$$\Delta E_g = 0 \quad \text{i.e., } \Delta n_i = 0 \quad (3.3c)$$

(iv) Homogeneity of temperature :

$$T = \text{constant over the whole body of the device} \quad (3.3d)$$

(v) No recombination and generation :

This forms the validity of the level 2 model for MOSFET.

$$R = 0 \quad (3.3e)$$

3.3 MODELLING OF THE PHYSICAL PARAMETERS :-

3.3a. Thermal voltage :

$$V_T = \frac{kT}{q} \quad (3.4)$$

where, k : Boltzmann's constant $= 1.381 \times 10^{-23}$ Joule/ $^{\circ}$ K

T : Absolute temperature ($^{\circ}$ K)

q : electronic charge $= 1.6 \times 10^{-19}$ coulomb .

3.3b. Intrinsic carrier concentration (n_i) :

$$n_i(T) = 3.88 \times 10^{16} T^{3/2} e^{(-7000/T)} \text{ (/cc)} \quad (3.5)$$

3.3c. Carrier Mobility :

Accurate mobility values are required for the purpose of predictive simulation because of the multiplicative dependence of

current upon mobility . Various mechanisms influence the carrier mobility ; they are scattering due to thermal vibration of lattice, ionized impurities, scattering of electron and hole, velocity saturation due to parallel electric field and the effect of transverse electric field etc .

There are several mobility models derived from theoretical background, approximately taking all the effects and their interactions . From simulation point of view, *empirical models* fit to the experimental data are of more importance . These type of models are used by several authors [Toyabe[17], Yamaguchi [20], Navon [21]] .

For the *thermal vibration of lattice*, mobility degradation is taken as a simple power law [tested and fit by Arora et al [22], Grove [23]] :

$$\mu_n^L = \mu_n^0 (T / 300^\circ K)^{-\alpha_n} \quad (3.6a)$$

$$\mu_p^L = \mu_p^0 (T / 300^\circ K)^{-\alpha_p} \quad (3.6b)$$

$$\begin{aligned} \text{where, } \mu_n^0 &= 1350 \text{ cm}^2/\text{v/s} & \alpha_n &= 2.5 \\ \mu_p^0 &= 480 \text{ cm}^2/\text{v/s} & \alpha_p &= 2.5 \end{aligned}$$

* The values are taken from Grove [23], similar expressions are supported in MINIMOS 1 [13] .

The empirical model including the effect of
(i) *impurity scattering*

(ii) velocity saturation at high electric field
(parallel to current flow) E_p &

(iii) surface scattering

was proposed by Yamaguchi [20], stated as :

$$\mu(N_B, E_p, E_T) = \mu^L \cdot f(N_B, E_p) \cdot g(E_T) \quad (3.7)$$

where, N_B : impurity concentration,

E_p : parallel electric field

E_T : transverse electric field, often referred as
'gate field'.

The term 'f' represent the bulk mobility reduction factor . This term was proposed by Scharfetter and Gummel [3] :

$$f(N_B, E_p) = \left[1 + \frac{N_B}{(N_B/S) + N} + \frac{(E_p/A)^2}{(E_p/A) + F} + (E_p/B)^2 \right]^{-1/2} \quad (3.8)$$

The first two terms account for impurity scattering mobility reduction. The constants S & N are explained in figure(3.1) . 'N' is the 'corner' impurity concentration where mobility reduction begins. \sqrt{S} is the maximum reduction of $\log(\mu)$.

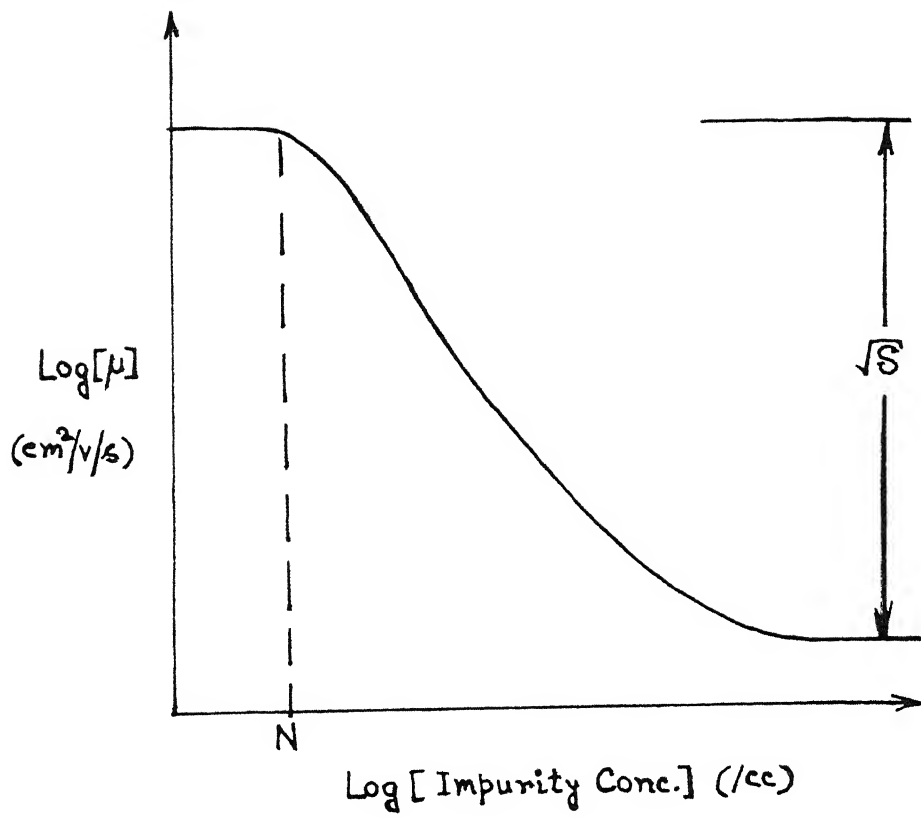


Fig. 3.1
Dependence of mobility on doping concentration
according to equation (3.8)

The values given by Scharfetter and Gummel [3] are :

	S	N (/cc)
Electron	350	$3 \cdot 10^{16}$
Hole	81	$4 \cdot 10^{16}$

* Table 3.1 *

The explanation of the last terms are given [Thornber [24]] by rearranging (3.8),

$$f(N_B, E_P) = \left[1 + \frac{N_B}{(N_B/S) + N} + (\mu^L)^2 \frac{(E_P / (\mu^L \cdot A))^2}{\mu^L \cdot E_P / (\mu^L \cdot A) + F} + \left[\frac{E_P}{\mu^L \cdot B} \right]^2 \right] \quad (3.9)$$

The term $(\mu^L \cdot B)$ represents the saturation velocity which is independent of impurity impurity scattering . The term $(\mu^L \cdot A)$ can be identified as acoustic phonon velocity, responsible for warm carriers. Here 'F' does not have any physical meaning, but a fitting factor of the empirical formula to the experimental

data .

The values of the constants at $T=300^{\circ}\text{K}$ [3] is tabulated in table(3.2).

	$A(\text{V/cm})$	F	$B(\text{V/cm})$
Electron	3.5×10^3	8.8	7.4×10^3
Hole	6.1×10^3	1.6	2.5×10^4

* Table 3.2 *

The temperature dependence of B and A constants given by Selberherr [25], used here :

$$B = 10^7 (T/300^{\circ}\text{K})^{-0.87} / \mu_n^L \quad \text{for electron} \quad (3.10a)$$

$$B = 8.37 \times 10^6 (T/300^{\circ}\text{K})^{-0.52} / \mu_p^L \quad \text{for hole} \quad (3.10b)$$

Temperature dependence of A is claimed [25] to be very weak, so its value in the table3.2 has been considered.

The 'g' term is introduced in (3.7), so as to represent the *surface mobility*. The carrier motion is strongly affected by the roughness of the surface and the interface states. The surface mobility decreases with the increase in gate field

[Fang & Fowler[26]]. An approximate formula which represents this property was proposed and established by Yamaguchi [20] .

$$g(E_T) = (1 + \alpha E_T)^{-1/2} \quad (3.11)$$

The parameter α is reciprocal of critical electric field .The value given by the same author as :

$$\alpha = \begin{cases} 1.539 \times 10^{-5} \text{ cm/v} & \text{for electron} \\ 5.35 \times 10^{-5} \text{ cm/v} & \text{for hole} \end{cases}$$

In the model (3.7) carrier-carrier scattering has not been taken into account . In the program, this effect has been included by a very simple approach [proposed by Engle and Dirks [27]], i.e., replacing N_B by :

$$N_B = 0.34 \text{ times doping concentration} + 0.66 \text{ times } (n+p) \quad (3.12)$$

The validity of these models used here are well established by the authors like Yamaguchi [20], Selberherr [25], Scharfetter and Gummel [3] and in several other papers.

3.3d. Doping profile :

Accurate doping can only be calculated by process simulation programs like SUPREM [28], SUPRA [29] etc.; these are

the problems of process modelling and simulation . In this device simulation program, implanted Gaussian doping profile in the source, drain and channel implantations has been assumed .

The vertical implanted Gaussian profile for source, drain and channel reads :

$$C(x) = \frac{\text{Dose}}{\sqrt{2\pi} \Delta R_p} \exp \left[- \frac{(x-R_p)^2}{2 \Delta R_p^2} \right] \quad (3.13)$$

where, Dose : implantation dose in atoms/cm²

R_p : projected range of implanted profile in cm

ΔR_p : straggle of the same in cm

For source and drain lateral diffusion exact profile can only be given by process simulation . An approximate Gaussian profile has been assumed in lateral direction :

$$C(x,y) = \frac{\text{Dose}}{\sqrt{2\pi} \Delta R_p} \exp \left[- \frac{(y-L_s)^2 + (x-R_p)^2}{2 \Delta R_p^2} \right] + \frac{\text{Dose}}{\sqrt{2\pi} \Delta R_p} \exp \left[- \frac{(y-(L_y-L_d))^2 + (x-R_p)^2}{2 \Delta R_p^2} \right] \quad (3.14)$$

where, L_s & L_d : Source & drain contact lengths

L_y : Lateral dimension of simulation area.

The values of R_p , ΔR_p are taken from graphs of these quantities against implantation energies (in KeV) [25].

Recombination generation has not been modelled as it has not been included in this simulation.

Chapter 4

NUMERICAL TREATMENT

The system of basic semiconductor equations cannot be solved explicitly taking all the non-ideal effects into account. Therefore, the solution must be calculated by means of numerical approaches. This chapter deals with these things.

4.1 BASIC CONCEPTS :-

The numerical approach for the solution of differential or partial differential equations, consists of essentially three tasks. First one is, the domain, i.e., simulation geometry of the device, has to be partitioned into a finite number of subdomains, in which the solution can be approximated with a desired accuracy. Secondly, the differential equations have to be approximated in each of the subdomains by algebraic equations which involve only values of the continuous dependent variables at discrete points. In this way, one obtains a fairly large system of algebraic equations with unknowns comprised of approximations of continuous dependent variables. The third task is to solve this system of equations.

It is to be mentioned here that the exact analytical solution cannot be found by the method outlined above. Rather, we get an exact solution of the system of algebraic equations. If the

subregions are small enough to ensure better fit to the exact values the numerical solution represents a good approximation to the solution of analytically formulated problems.

There are many classical methods which propose the possibility of the partitioning of the domain (discretization). The are :

- (i) Finite Difference Method (F.D.M.)
- (ii) Finite Box Method (generalized F.D.M.)
- (iii) Finite element Method (F.E.M.).

We used F.D.M. discretization as it is easier to tackle regular shaped geometry like that of MOSFET, than other methods.

4.2 GRID FORMATION :-

In F.D.M. the domain is discretized by straight lines (grids or mesh) parallel to X and Y axes. The spacing is kept non-uniform, closely spaced grids are used where there is a chance of the variation of any dependent variable to be stiff, and where the variation is less, grids are spaced widely apart. (More about the generation of non-uniform grid or mesh is discusses later.). One possible grid-structure is shown if Figure 4.1; it is used as the starting mesh in this program. There are NX lines in X-direction, NY in Y-direction, so there are (NX.NY) grid points, where we have to approximate the analytical differential equations.

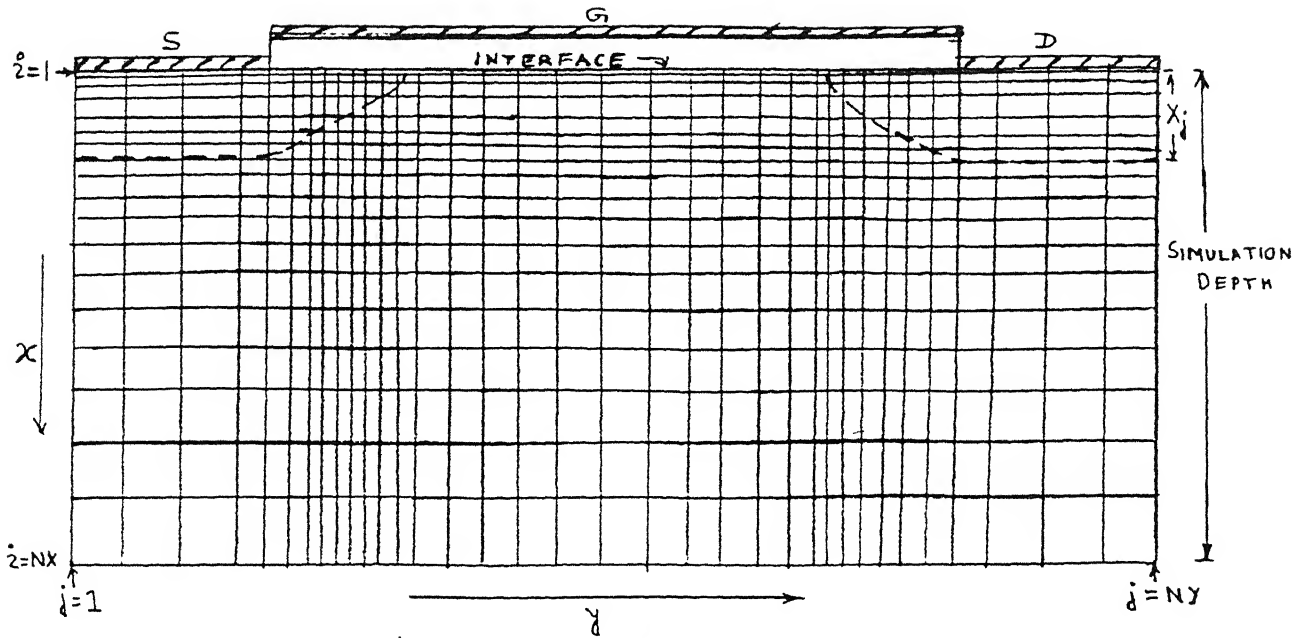


Fig. 4.1
The non-uniform grid used in the finite difference scheme

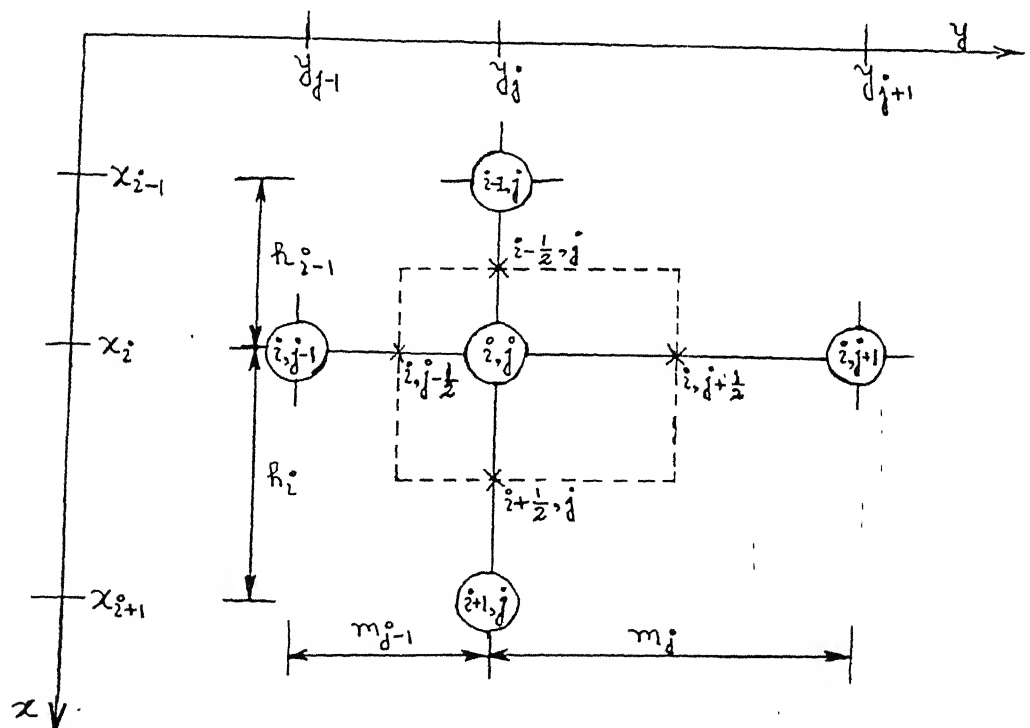


Fig. 4.2
The five point molecule used in the finite difference discretization

4.3 DISCRETIZATION :-

Here, the differential equations are replaced by difference equations on the grid points by suitable discretization techniques [30], [31].

We used five point molecule (Figure 4.2) for the discretization of the 2-d partial differential equations (the basic equations discussed in the previous chapter).

The notations used in the discretization are given as follows:

Grid spacings :

$$h_i = x_{i+1} - x_i ; \quad i = 1 \text{ to } NX - 1 \quad (4.1a)$$

$$m_j = y_{j+1} - y_j ; \quad j = 1 \text{ to } NY - 1 \quad (4.1b)$$

Discrete point dependent variables :

$$f_{i,j} = f(x_i, y_j); \quad i = 1 \text{ to } NX, \quad j = 1 \text{ to } NY \quad (4.2a)$$

$$f_{i+1/2,j} = f\left(\frac{x_i + x_{i+1}}{2}, y_j\right); \quad i = 1 \text{ to } NX, \quad j=1 \text{ to } NY \quad (4.2b)$$

$$f_{i,j+1/2} = f\left(x_i, \frac{y_j + y_{j+1}}{2}\right); \quad i = 1 \text{ to } NX, \quad j=1 \text{ to } NY \quad (4.2c)$$

Where, 'f' is any one of the dependent variables ψ , n or p ; physical parameters C (doping density), γ_n or γ_p (normalized

mobility) or parameters like E (electric field), current density J_n or J_p .

4.3a Discretization of Poisson's Equation :-

In 2-D simulation, we assumed MOS with large width (W) and no variation of any of the dependent variables in Z-direction (normal to the paper). Hence the normalized Poisson's equation becomes as:

$$\begin{aligned}\frac{\partial^2 \psi}{\partial x^2} + \frac{\partial^2 \psi}{\partial y^2} &= (e^{\psi - \phi_n} - e^{\phi_p - \psi} - C) \\ &= (n - p - C)\end{aligned}\quad (4.3)$$

It is linearized by Newton's method [1], assuming,

$$\psi_{\text{exact}} = \psi + \alpha \quad (4.4a)$$

$$e^{\pm \alpha} \simeq 1 \pm \alpha \quad (4.4b)$$

Where, α is very small quantity, defined as the error in potential when we approximate (4.3) as linear one.

With the assumptions (4.4a) and (4.4b), Poisson's equation is linearized down to :

$$\frac{\partial^2 \alpha}{\partial x^2} + \frac{\partial^2 \alpha}{\partial y^2} - \alpha(n+p) = (n - p - C) - \left[\frac{\partial^2 \psi}{\partial x^2} + \frac{\partial^2 \psi}{\partial y^2} \right] \quad (4.5)$$

The Poisson's equation is solved iteratively by making a guess at K-th iteration for ψ , α is calculated from (4.5), the guess is refined as (4.6) and proceed to K+1st iteration.

$$\psi^{K+1} = \psi^K + \alpha^K \quad (4.6)$$

This is iterated until α^K becomes negligible.

Now referring to Figure 4.2 of non-uniform 5 point molecule, ψ is expanded in Taylor's series about the points $(i+1/2, j)$ and $(i-1/2, j)$ and subtracting these expansions, we get after rearrangement,

$$\left(\frac{\partial \psi}{\partial x}\right)_{i,j} = \frac{\psi_{i+1/2,j} - \psi_{i-1/2,j}}{\frac{h_i + h_{i-1}}{2}} + O(h) \left(\frac{\partial^2 \psi}{\partial x^2}\right)_{i,j} + O(h^2) \left(\frac{\partial^3 \psi}{\partial x^3}\right)_{i,j} + \dots \quad (4.7)$$

where, $O(h)$: of order $h = \frac{h_i - h_{i-1}}{4}$

$$O(h^2): \text{ of order } h^2 = \frac{(h_i^3 - h_{i-1}^3)/24}{(h_i - h_{i-1})/2} \text{ etc.} \quad (4.8)$$

Similarly, analogous expressions can be derived for $\left(\frac{\partial \psi}{\partial y}\right)_{i,j}$, $\left(\frac{\partial \alpha}{\partial x}\right)_{i,j}$, $\left(\frac{\partial \alpha}{\partial y}\right)_{i,j}$.

Using (4.7) and its analogues in (4.5) we get,

$$\begin{aligned}
& \left[\frac{\left(\frac{\partial \alpha}{\partial x} \right)_{i+1/2, j} - \left(\frac{\partial \alpha}{\partial x} \right)_{i-1/2, j}}{\frac{h_i + h_{i-1}}{2}} + O(h) \left(\frac{\partial^3 \alpha}{\partial x^3} \right)_{i, j} \right. \\
& \left. + \frac{\left(\frac{\partial \alpha}{\partial y} \right)_{i, j+1/2} - \left(\frac{\partial \alpha}{\partial y} \right)_{i, j-1/2}}{\frac{m_j + m_{j-1}}{2}} + O(m) \left(\frac{\partial^3 \alpha}{\partial y^3} \right)_{i, j} \right] - \alpha_{i, j} (n_{i, j} + p_{i, j}) \\
& = (n_{i, j} + p_{i, j} + c_{i, j}) - \left[\frac{\left(\frac{\partial \psi}{\partial x} \right)_{i+1/2, j} - \left(\frac{\partial \psi}{\partial x} \right)_{i-1/2, j}}{\frac{h_i + h_{i-1}}{2}} + O(m) \left(\frac{\partial^3 \psi}{\partial x^3} \right)_{i, j} \right. \\
& \left. + \frac{\left(\frac{\partial \psi}{\partial y} \right)_{i, j+1/2} - \left(\frac{\partial \psi}{\partial y} \right)_{i, j-1/2}}{\frac{m_j + m_{j-1}}{2}} + O(m) \left(\frac{\partial^3 \psi}{\partial y^3} \right)_{i, j} \right] \quad (4.9)
\end{aligned}$$

Next. we derive as equation (4.7) for $\left(\frac{\partial \psi}{\partial x} \right)_{i+1/2, j}$, $\left(\frac{\partial \alpha}{\partial x} \right)_{i+1/2, j}$ etc.

$$\left(\frac{\partial \psi}{\partial x} \right)_{i+1/2, j} = \frac{\psi_{i+1, j} - \psi_{i, j}}{h_i} + O(h^2) \left(\frac{\partial^3 \psi}{\partial x^3} \right)_{i+1/2, j} + \dots \quad (4.10)$$

and so on.

We assume, h_i and m_j are small enough to make the effect of $O(h)$ or $O(m)$ times the third derivative of potential and similar higher order terms negligible [they are called the local truncation errors]. Combining (4.9) with (4.10) and its analogues, we get the difference equation for linearized and normalized Poisson's equation [excluding local truncation errors] as follows :

$$\begin{aligned}
& \left[\frac{\frac{\alpha_{i+1,j} - \alpha_{i,j}}{h_i} - \frac{\alpha_{i,j} - \alpha_{i-1,j}}{h_{i-1}}}{\frac{h_i + h_{i-1}}{2}} + \frac{\frac{\alpha_{i,j+1} - \alpha_{i,j}}{m_j} - \frac{\alpha_{i,j} - \alpha_{i,j-1}}{m_{j-1}}}{\frac{m_j + m_{j-1}}{2}} \right] \\
& - \alpha_{i,j} (n_{i,j} + p_{i,j}) = (n_{i,j} - p_{i,j} - C_{i,j}) - \\
& \left[\frac{\frac{\psi_{i+1,j} - \psi_{i,j}}{h_i} - \frac{\psi_{i,j} - \psi_{i-1,j}}{h_{i-1}}}{\frac{h_i + h_{i-1}}{2}} + \frac{\frac{\psi_{i,j+1} - \psi_{i,j}}{m_j} - \frac{\psi_{i,j} - \psi_{i,j-1}}{m_{j-1}}}{\frac{m_j + m_{j-1}}{2}} \right]
\end{aligned} \tag{4.11}$$

Local truncation errors (L.T.E.) in the difference equation (4.11) are as :

Truncation error in α (dropping subscripts)

$$T_{\alpha} \leq O(h) \left| \frac{\partial^3 \alpha}{\partial x^3} \right| + O(m) \left| \frac{\partial^3 \alpha}{\partial y^3} \right| \tag{4.12}$$

L.T.E. in ψ is just similar to (4.12), with α replaced by ψ .

From equation (4.12) it is clear that, L.T.E. is linearly proportional to the grid spacing. So, closely spaced grid is to be set, where ψ (so α) varies sharply to get better approximation to exact solution. Widely spaced grids are used where ψ varies very little (in the bulk of MOS) so as to decrease the number of grid points (to minimize C.P.U. time on computation).

One important point is to be noted here; by comparing equation (4.5) and difference equation (4.11) one can conclude

that ψ (and α also) is taken to be varying linearly between two neighbouring grid points, during the derivation of difference equation.

Now, we derive the difference equation for Poisson's equation at the boundaries.

(i) At the ohmic contacts of source, drain and gate, ψ is known as

$$\psi = V_{\text{applied}} + V_{\text{built in}} \quad (4.12)$$

So ψ_{exact} is known and from equation (4.4a), it is clear that

$$\alpha = 0 \quad (4.13)$$

Setting this condition in equation (4.11) we get difference equation at ohmic contacts.

(ii) At the fictitious boundaries [$j = 1$ & NY and $X_i =$ simulation depth], we assumed in chapter 2 that no electric field is going out of the device :

$$\frac{\partial \psi}{\partial y} + \frac{\partial \alpha}{\partial y} = 0 \text{ at } j = 1 \text{ \& \> } NY \text{ for } 1 \leq i \leq NX \quad (4.14a)$$

Replacing it by difference approximation,

$$\frac{\psi_{i,j+1/2} - \psi_{i,j-1/2}}{\frac{m_j + m_{j-1}}{2}} + \frac{\alpha_{i,j+1/2} - \alpha_{i,j-1/2}}{\frac{m_j + m_{j-1}}{2}} = 0 \quad (4.14b)$$

As m_{j-1} is outside point for $j = 1$ and m_j is so for $j = NY$, we use,

$$m_j = m_{j-1} \quad (4.14c)$$

$$\text{and } \psi_{i,j\pm 1/2} = \frac{\psi_{i,j\pm 1} - \psi_{i,j}}{2} \quad (4.14d)$$

From equation (4.14b), (4.14c) and (4.14d) we get

$$\psi_{i,j-1} + \alpha_{i,j-1} = \psi_{i,j+1} + \alpha_{i,j+1} \quad (4.14e)$$

Similarly, for x_i = simulation depth

$$\psi_{i+1,j} + \alpha_{i+1,j} = \psi_{i-1,j} + \alpha_{i-1,j} \quad (4.14f)$$

By equation (4.14e) and (4.14f) we replace points outside domain in equation (4.11). This method is called image point technique.

(iii) Now comes the interface between Si and SiO₂, under gate. Special care is taken in discretizing the Poisson's equation at interface.

Boundary condition for interface is given by equation (2.16) of chapter 2. It is rewritten for discretization here,

$$\epsilon_{Si} \left[-\frac{\partial \psi}{\partial x} - \frac{\partial \alpha}{\partial x} \right]_{Si} = \epsilon_{ox} \left[-\frac{\partial \psi}{\partial x} - \frac{\partial \alpha}{\partial x} \right]_{SiO_2} + Q_{INT} \quad (4.15)$$

at $i = 1$ under gate.

Expanding the point (i, j) about $(i+1/2, j)$ and using equation (4.5), we get,

$$\begin{aligned} \left\{ \frac{\partial \psi}{\partial x} + \frac{\partial \alpha}{\partial x} \right\}_{i,j|Si} &= - \left\{ \frac{\partial \psi}{\partial x} + \frac{\partial \alpha}{\partial x} \right\}_{i+1/2,j} + \frac{h_i}{2} \left\{ \frac{\partial^2 \psi}{\partial x^2} + \frac{\partial^2 \alpha}{\partial x^2} \right\}_{i,j|Si} \\ &= - \left\{ \frac{\partial \psi}{\partial x} + \frac{\partial \alpha}{\partial x} \right\}_{i+1/2,j} + \frac{h_i}{2} \left[- \frac{\partial^2 \psi}{\partial y^2} - \frac{\partial^2 \alpha}{\partial y^2} + (n-p-C) \right. \\ &\quad \left. + \alpha(n+p) \right]_{i,j|Si} \end{aligned} \quad (4.16a)$$

Similarly expanding (i, j) about $(i-1/2, j)$

$$\left\{ \frac{\partial \psi}{\partial x} + \frac{\partial \alpha}{\partial x} \right\}_{i,j|SiO_2} = - \left\{ \frac{\partial \psi}{\partial x} + \frac{\partial \alpha}{\partial x} \right\}_{i-1/2,j} + \frac{h_{i-1}}{2} \left\{ \frac{\partial^2 \psi}{\partial x^2} + \frac{\partial^2 \alpha}{\partial x^2} \right\}_{i,j|SiO_2} \quad (4.16b)$$

The point $(i-1/2, j)$ is inside the oxide where Laplace Equation is valid,

$$\left(\frac{\partial^2}{\partial x^2} + \frac{\partial^2}{\partial y^2} \right) (\psi + \alpha) = 0 \quad (4.16c)$$

Since, oxide thickness (t_{ox}) is very small, one dimensional linear potential drop inside the oxide is considered. So, the 1st term in the r.h.s. of equation (4.16b) is approximated by

$$- \frac{\partial \psi}{\partial x} - \frac{\partial \alpha}{\partial x} = \frac{\psi_G - \psi_{i,j} - \alpha_{i,j}}{t_{ox}} \quad (4.16d)$$

where

$$\psi_G = V_{G(\text{applied})} - V_{\text{Flat Band}} \quad (4.16e)$$

$$\text{and } V_{\text{Flat Band}} = \phi_{\text{MS}} - \frac{Q_{\text{INT}}}{C_{\text{ox}}} \quad (4.16f)$$

where, ϕ_{MS} : Gate metal - Semiconductor work function difference
 C_{ox} : Gate oxide capacitance

With this definition of ψ_G , we don't need to treat Q_{INT} in equation (4.15) separately, we drop this term from equation (4.15) and proceed. Using equation (4.16d) and Laplace equation, we get,

$$-\left\{\frac{\partial\psi}{\partial x} + \frac{\partial\alpha}{\partial x}\right\}_{i,j|\text{SiO}_2} = \frac{\psi_G - \psi_{i,j} - \alpha_{i,j}}{t_{\text{ox}}} - \frac{t_{\text{ox}}}{2} \left[-\frac{\partial^2\psi}{\partial y^2} - \frac{\partial^2\alpha}{\partial y^2} \right]_{i,j|\text{SiO}_2} \quad (4.16g)$$

Now, we put equation (4.16a) and equation (4.16g) in modified equation (4.15) [Q_{INT} is dropped with ψ_G definition], and we get after discretizing $\frac{\partial^2\psi}{\partial x^2}$ etc. terms as done earlier, the difference equation at interface :

$$\begin{aligned}
& \left[\frac{\frac{\alpha_{i,j+1} - \alpha_{i,j}}{m_j} - \frac{\alpha_{i,j} - \alpha_{i,j-1}}{m_{j-1}}}{\frac{m_j + m_{j-1}}{2}} \right] + \left[\frac{\frac{\psi_{i,j+1} - \psi_{i,j}}{m_j} - \frac{\psi_{i,j} - \psi_{i,j-1}}{m_{j-1}}}{\frac{m_j + m_{j-1}}{2}} \right] \\
& + \frac{\frac{\epsilon_{Si} \frac{\alpha_{i+1,j} - \alpha_{i,j}}{h_i} - \epsilon_{ox} \frac{\alpha_{i,j}}{t_{ox}}}{\epsilon_{Si} h_i + \epsilon_{ox} t_{ox}}}{2} + \frac{\frac{\epsilon_{Si} \frac{\psi_{i+1,j} - \psi_{i,j}}{h_i} - \epsilon_{ox} \frac{\psi_{i,j} - \psi_G}{t_{ox}}}{\epsilon_{Si} h_i + \epsilon_{ox} t_{ox}}}{2} \\
& - \frac{\epsilon_{Si} h_i}{(\epsilon_{Si} h_i + \epsilon_{SiO_2} t_{ox})} (n_{i,j} + p_{i,j}) \alpha_{i,j} = \frac{h_i}{t_{ox} \epsilon_{ox}} (n_{i,j} - p_{i,j} - C_{i,j}) \\
& \quad \quad \quad \frac{h_i}{h_i + \frac{\epsilon_{Si}}{\epsilon_{SiO_2}}}
\end{aligned}$$

[at $i = 1$, $j \equiv$ under gate]

(4.17)

4.3b Discretization of Continuity Equation :-

The major difficulty of the discretization of continuity equation is to find a proper numerically stable formulation using only the information at the mesh points. The naive discretization proposed by Van Dorpe [4] has been proved to be unstable [3], [8], [32]. It is also tested by this program, and is found to be very prone to overflow traps and inconsistent solution when large voltage is applied and mesh spacing is not very close. It is clear from difference scheme of Poisson's equation that ψ is interpolated linearly between neighbouring mesh points. A naive linear interpolation (used in [4]) of n and p is surely inappropriate as n and p vary as the exponential of ψ , unless the variation of ψ between mesh points is less $2KT/q$ [3].

So, we've chosen the discretization scheme proposed by Scharfetter and Gummel [3]. Although, they have proposed it for one-dimensional Read-diode oscillator, it is extended to 2-D as per the requirement of the simulation here.

The outline for discretizing the continuity equation for electron is discussed here for hole it can be derived analogously.

The normalized electron current density expression reads

$$J_n = \gamma_n n(-\nabla\psi) + \gamma_n \nabla n \quad (4.18)$$

Where γ_n is normalized mobility, $\gamma_n = \mu_n/\mu_o$

J_n is broken in two orthogonal components,

$$J_n = J_{nx} + J_{ny} \quad (4.19a)$$

where,

$$J_{nx} = \gamma_n n\left(-\frac{\partial\psi}{\partial x}\right) + \gamma_n \frac{\partial n}{\partial x} \quad (4.19b)$$

$$J_{ny} = \gamma_n n\left(-\frac{\partial\psi}{\partial y}\right) + \gamma_n \frac{\partial n}{\partial y} \quad (4.19c)$$

Now, we start our derivation with equation (4.19a) rewritten as,

$$\gamma_n \left(\frac{\partial n}{\partial x}\right) + \gamma_n E_n = J_{nx} \quad (4.20)$$

$$\text{where, } E = - \frac{\partial \psi}{\partial x} \quad (4.21)$$

We concentrate, on the path between two mesh points (i, j) and $(i+1, j)$ as shown in figure 4.3.

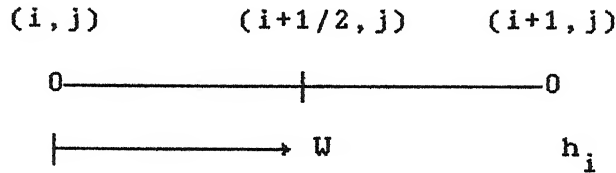


Figure 4.3

W : a local variable at $x = x_i$, $W = 0$ and at $x = x_{i+1}$, $W = h_i$ and $\frac{\partial}{\partial x} = \frac{\partial}{\partial W}$

If we consider E , γ_n and J_{n_x} to be constant to the mid-vertex $(i+1/2, j)$ value over this path, equation (4.20) becomes a Leibnitz differential equation as,

$$\frac{\partial n}{\partial W} + E_{i+1/2, j} n = \frac{J_{n_x i+1/2, j}}{\gamma_{n i+1/2, j}} \quad (4.22)$$

with boundary conditions,

$$\begin{aligned} \text{at } W = 0 & \quad , \quad n = n_{i, j} \\ \text{at } W = h_i & \quad , \quad n = n_{i+1/2, j} \end{aligned} \quad (4.23)$$

Solution of equation (4.22) (without Boundary condition):

$$n e^{\int E_{i+1/2, j} dW} = \int \frac{J_{n_x i+1/2, j}}{\gamma_{n i+1/2, j}} e^{\int E_{i+1/2, j} dW} + C \quad (4.24a)$$

Where, C is a constant and evaluated by equation (4.23) and rearranging the final expression, we get,

$$J_{nx_{i+1/2,j}} = \gamma_{n_{i+1/2,j}} E_{i+1/2,j} \left[\frac{n_{i+1,j}}{1 - \exp(-E_{i+1/2,j} h_i)} + \frac{n_{i,j}}{1 - \exp(+E_{i+1/2,j} h_i)} \right] \quad (4.24b)$$

Equation (4.21) discretized as :

$$E_{i+1/2,j} = \frac{\psi_{i,j} - \psi_{i+1,j}}{h_i} \quad (4.24c)$$

Combining equation (4.24b) and equation (4.24c), we get,

$$J_{nx_{i+1/2,j}} = \frac{\gamma_{n_{i+1/2,j}}}{h_i} \left[n_{i+1,j} B(\psi_{i+1,j} - \psi_{i,j}) - n_{i,j} B(\psi_{i,j} - \psi_{i+1,j}) \right] \quad (4.25)$$

where, $B(t) = \frac{t}{e^t - 1}$: Bernouli function

Similar will be the expressions for $J_{nx_{i-1/2,j}}$ $J_{ny_{i,j+1/2}}$ and $J_{ny_{i,j-1/2}}$

Now, we consider the steady state continuity equation for electron,

$$\frac{\partial J_{nx}}{\partial x} + \frac{\partial J_{ny}}{\partial y} = R \quad (4.26)$$

[In this simulation we neglect R , as the MOS not in breakdown, for the shake of completeness we keep R here].

Discretizing equation (4.26) as done in case of Poisson's equation,

$$\begin{aligned} & \frac{J_{nx_{i+1/2,j}} - J_{nx_{i-1/2,j}}}{\frac{h_i + h_{i-1}}{2}} + O(h) \left(\frac{\partial J_{nx}}{\partial x} \right)_{i,j} \\ & + \frac{J_{ny_{i,j+1/2}} - J_{ny_{i,j-1/2}}}{\frac{m_j + m_{j-1}}{2}} + O(m) \left(\frac{\partial J_{ny}}{\partial y} \right)_{i,j} = R_{i,j} \quad (4.27) \end{aligned}$$

Neglecting L.T.E. of order $O(h)$, $O(K)$ in equation (4.27) and combining equation (4.25) and similar expressions, we get,

$$\begin{aligned} & \gamma_{n_{i+1/2,j}} \frac{n_{i+1,j} B(\psi_{i+1,j} - \psi_{i,j}) - n_{i,j} B(\psi_{i,j} - \psi_{i+1,j})}{\frac{h_i(h_i + h_{i-1})}{2}} \\ & - \gamma_{n_{i-1/2,j}} \frac{n_{i,j} B(\psi_{i,j} - \psi_{i-1,j}) - n_{i-1,j} B(\psi_{i-1,j} - \psi_{i,j})}{\frac{h_{i-1}(h_i + h_{i-1})}{2}} \\ & + \gamma_{n_{i,j+1/2}} \frac{n_{i,j+1} B(\psi_{i,j+1} - \psi_{i,j}) - n_{i,j} B(\psi_{i,j} - \psi_{i,j+1})}{\frac{m_j(m_j + m_{j-1})}{2}} \\ & - \gamma_{n_{i,j-1/2}} \frac{n_{i,j} B(\psi_{i,j} - \psi_{i,j-1}) - n_{i,j-1} B(\psi_{i,j-1} - \psi_{i,j})}{\frac{m_{j-1}(m_j + m_{j-1})}{2}} \\ & = R_{i,j} \quad (4.28) \end{aligned}$$

where,

$$\gamma_{n_{i+1/2},j} \approx \frac{1}{2} (\gamma_{n_{i+1},j} + \gamma_{n_i,j}) \quad (4.29)$$

and L.T.E. in equation (4.28) is

$$T_n \leq O(h) \left| \frac{\partial J_{nx}}{\partial x} \right| + O(m) \left| \frac{\partial J_{ny}}{\partial y} \right| \quad (4.30)$$

Analogously, difference equation for hole continuity equation can be derived and the final form of equation will be same as equation (4.28), except $n_{i,j}$'s are replaced by $p_{i,j}$'s, subscript of γ is changed to p and the argument of Bernouli function are multiplied by -1 .

Now, boundary condition for continuity equation is to be imposed.

(i) At the ohmic contacts, n and p are known from equation (2.17).

(ii) At the fictitious boundaries we use image point technique to eliminate points outside simulation domain, as :

$$n_{i,j-1} = n_{i,j+1} ; p_{i,j-1} = p_{i,j+1} \text{ at } j = 1 \text{ and } NY \quad (4.31a)$$

$$\text{and } n_{i+1,j} = n_{i-1,j} ; p_{i+1,j} = p_{i-1,j} \text{ at } i = NX \quad (4.31b)$$

(iii) At the interface :-

We impose no current component normal to the interface, equation (2.18) reads :

$$J_{nx} = 0 \text{ and } J_{px} = 0 \text{ at } i = 1, j : \text{ under gate}$$

Without the loss of generality, we assume, $h_i = h_{i-1}$, as h_{i-1} is fictitious at $i = 1$, and we write (for electron)

$$J_{nx_{i,j}} = \frac{J_{nx_{i+1/2,j}} + J_{nx_{i-1/2,j}}}{2} \quad (4.32)$$

As $J_{nx_{i,j}} = 0$ at $i = 1$, J : under gate, equation (4.32) implies,

$$J_{nx_{i-1/2,j}} = - J_{nx_{i+1/2,j}} \quad (4.33)$$

Combining equation (4.33), (4.27) and (4.25) and similar expressions, we get

$$\begin{aligned} & 2\gamma_{n_{i+1/2,j}} \frac{[n_{i+1,j} B(\psi_{i+1,j} - \psi_{i,j}) - n_{i,j} B(\psi_{i,j} - \psi_{i+1,j})]}{h_i^2} \\ & + \gamma_{n_{i,j+1/2}} \frac{n_{i,j+1} B(\psi_{i,j+1} - \psi_{i,j}) - n_{i,j} B(\psi_{i,j} - \psi_{i,j+1})}{\frac{m_j(m_j + m_{j-1})}{2}} \\ & - \gamma_{n_{i,j-1/2}} \frac{n_{i,j} B(\psi_{i,j} - \psi_{i,j-1}) - n_{i,j-1} B(\psi_{i,j-1} - \psi_{i,j})}{\frac{m_{j-1}(m_j + m_{j-1})}{2}} \\ & = R_{i,j} \end{aligned} \quad (4.34)$$

The difference equation for hole continuity equation at interface is analogous.

4.4 COMPUTER IMPLEMENTATION OF BERNOULI FUNCTION :-

The Bernouli function used in discretizing continuity equations, defined as,

$$B(t) = \frac{t}{e^t - 1} \quad (4.35)$$

In the actual programming of $B(t)$ special care is taken to avoid floating point overflow and underflow traps. it is clear from equation (4.35), at $t = 0$, $B(0)$ gives divide by zero error at $t \gg 1$ and $t \ll 0$ exponential terms may give overflow and underflow error. So Bernouli function is implemented as suggested by Hart, Cheney, Lauson and Maehly [33], [25]. This implementation is basically defining $B(t)$ by different expressions at different ranges of t ,

$$B(t) = \begin{cases} -t & \text{when } t \leq t_1 \\ \frac{t}{e^t - 1} & \text{when } t_1 < t < t_2 \\ 1 - t/2 & \text{when } t_2 \leq t \leq t_3 \\ \frac{t e^{-t}}{1 - e^{-t}} & \text{when } t_3 < t < t_4 \\ t e^{-t} & \text{when } t_4 \leq t \leq t_5 \\ 0 & \text{when } t_5 \leq t \end{cases} \quad (4.36)$$

The constants t_1 to t_5 depend on individual computer hardware. They are defined by :-

$$\text{For } t_1, \quad e^{t_1} - 1 \text{ '}' - 1 \quad (4.37a)$$

$$\text{For } t_2, \quad \frac{e^{t_2}}{e^{t_2} - 1} \text{ '}' 1 - \frac{t_2}{2}, \quad [t_2 < 0] \quad (4.37b)$$

$$\text{For } t_3, \quad 1 - \frac{t_3}{2} \text{ '}' \frac{t_3 e^{-t_3}}{1 - e^{-t_3}}, \quad [t_3 > 0] \quad (4.37c)$$

$$\text{For } t_4, \quad 1 - e^{-t_4} \text{ '}' 1 \quad (4.37d)$$

$$\text{For } t_5, \quad e^{-t_5} \text{ '}' 0 \quad (4.37e)$$

The equal to (=) sign is quoted to mean that it is not mathematically equal, but the numerical values calculated by the computer are equal on both sides of the equations (3.38a...e).

The constants evaluated for HP 9000 computer are as :-

$$t_1 \simeq -14.4954662$$

$$t_2 \simeq -0.650278232 \times 10^{-2}$$

$$t_3 \simeq +0.6083747372 \times 10^{-2}$$

$$t_4 \simeq 14.4954662$$

$$t_5 \simeq 87.3300171$$

4.5 ADAPTIVE GRID GENERATION :-

As the discretization errors depend on the distribution of the quantities ψ , n , p , a suitable mesh cannot be estimated a priori, i.e., without the knowledge of the solution. Therefore, grid generation is performed adaptively, a preliminary solution is calculated on the basis of an initial mesh (in sec. 4.2), then the mesh is adapted to this solution and again basic equation are solved. Re-generation of mesh is repeated whenever necessary. It is to be mentioned here that, the preliminary solution of basic equation need not be very accurate solution; it, even, may be the initial guess followed by solution of poisson's equation and p & n adjustment.

An easy method, used in adapting the mesh is described below :- From theory we know ψ varies as an exponential function of spatial coordinate away from the interface of Si - SiO₂ when there is a gate voltage. The function is crudely of the form (only x-variation) :-

$$\psi(x) = A e^{-Bx} \quad (4.38)$$

where A , B are constants.

Expanding equation (4.38) about neighbouring mesh point, we get, after some rearrangement,

$$\frac{\psi(x+h) - \psi(x)}{\psi(x)} = -hB + \frac{h^2 B^2}{2} \quad (4.39)$$

We use L.H.S. of equation (4.39) as maximum relative error ϵ_{MAX} . The 1st term R.H.S. of (4.39) describes the variation as linear one between two mesh points; this assumption is made during discretization of Poisson's equation (Sec. 4.3). So the local error in linear interpolation of ψ is given by $|h^2 B^2 / 2|$.

$$\epsilon_{\text{max}} = \frac{h^2 B^2}{2} \quad (4.40a)$$

Now (hB) is calculated from equation (4.40a) and feed to equation (4.40b)[derived from equation (4.38)],

$$\frac{\psi(x) - \psi(x + h)}{\psi(x)} = 1 - e^{-hB} \quad (4.40b)$$

Equation (4.40a) and equation (4.40b) gives an estimate of maximum allowed fractional change in normalized ψ between mesh points, for which local error is less than ϵ_{MAX} . For $\epsilon_{\text{MAX}} \simeq 10^{-3}$, fractional change in normalized is calculated to be 4.39%. Quantitatively speaking, if we apply 6V at the maximum and built in potential is within 0.9V, then one grid is to be inserted whenever there is change of 11.6 thermo-volt between mesh points.

In discretization of continuity equations (Sec. 4.3b), we considered the variation of ψ linear between mesh points, so this rule of grid adaptation is valid for n and p distribution also.

The initial coarse grid is generated accounting for the bias values, doping profile and important boundaries.

In x-direction, Si - SiO₂ boundary is very important, as inversion layer (if formed) is limited within few thermo - voltage

fall from interface. So, I used 1st grid spacing as the depth within which ψ drops by one thermo-voltage. Then spacing increases exponentially as we move away from surface.

In y-direction, fictitious vertical boundaries are prone to large local truncation errors, so y-grids are closely spaced there. To track the lateral diffusion of source and drain, grids are inserted for every 100/CC fall in doping concentration. this thing is done in x-direction upto the junction depths. The initial grid spacing is sinusoidally varying in the effective channel.

In this way minimum number of grids (18 x 20) for a particular case, and maximum allowable grid adaptation is done upto (49 x 49).

Chapter 5

ALGORITHMS TO EXTRACT RESULTS

In the preceding chapter, three coupled semiconductor equations are linearized as required and discretized. A large system of linear simultaneous algebraic equations, with the values of the dependent variables of the differential equations at discrete points as unknowns, are obtained. Direct solution of this system becomes impossible. For example, if grid points are $N_x.N_y = 20 \times 20$, the number of unknowns becomes $\{3(N_x.N_y)\}$ and the size of the coefficient matrix will be $3(N_x.N_y)$ times $3(N_x.N_y)$. Which amounts to (1200, 1200) at the minimum number grids.

To solve this large system, GUMMEL'S ALGORITHM [1] is popularly used in device simulation.

5.1 GUMMEL'S ALGORITHM :-

5.1.a The Basic Idea :

Gummel's idea was, in essence, to solve the coupled semiconductor equations by independently solving each equation, assuming the knowledge of the result of the other equations. The steps involved are as follows :

- (i) Prepare initial guess for ψ , n and p .
- (ii) Assuming knowledge of ψ to be exact, solve discretized electron continuity equation to get better approximation to n
- (iii) Assuming knowledge ψ to be exact, solve discretized hole continuity equation to get better approximation to p .

(iv) Now, assuming knowledge of p and n from steps (ii) and (iii) to be exact, Poisson's equation is solved, to get better approximation to ψ .

(v) Test the convergence and eventually return to step (ii).

The effort to solve for one cycle of this iteration, is obviously less than any other solution methods like Newton's method, because the rank of the matrix for one decoupled equation is one-third of the rank of the total system.

5.1.b Convergence :

A complete theoretical proof for the convergence of the algorithm has not been published yet. However, strong theoretical indication has been given by Mock [35]. The "practical" value of this algorithm is not underestimated, many authors [Vandorpe [4], Scharfetter and Gummel [3], Mock [6], Selberherr et al. [13], De la Moneda [19] and several others] have used Gummel's algorithm with excellent success as they claimed.

5.1.c Modification :

Gummel's algorithm is slightly modified and simplified for level 2 model [Sec. 3.1], used in this simulation. In level 2, only majority carrier continuity equation is solved. So, any one of the steps, (ii) or (iii), is replaced by corresponding minority carrier adjustment, as:

$$n^{K+1} = n^K \exp(\alpha^{K+1}) \quad (5.1a)$$

$$\text{or, } p^{K+1} = p^K \exp(-\alpha^{K+1}) \quad (5.1b)$$

where, superscript k is the value at K -th iteration, and α is error in ψ as described ago, and ψ is adjusted as

$$\psi^{K+1} = \psi^K + \alpha^K \quad (5.1c)$$

5.1.d Initial Guess :

In strong inversion region it is reported, the decoupled system needs 200 or more iteration [16], [19]. One reason for this, is due to the strong coupling between continuity and Poisson's equations, under strong inversion. Other reason is the large error in the initial guess. It has also been tested in this simulation program that crude initial guess, sometimes caused divergence and floating point overflow. So, extensive care is taken in the preparation of the initial guess. For, the uniqueness of the solution [Mock [34]], specified initial data (ψ , n , p) which fulfill the Poisson's equation is necessary.

Figure 5.1 shows the flow chart of initial guess preparation. Increment in the terminal bias is set $20V_T$ by trial and error method to avoid over flow in equation (5.1a) and equation (5.1b), if increment is greater than final bias value, directly final bias is set.

Figure 5.2 in flow chart for modified Gummel's algorithm, for a single operating point. For calculating I-V characteristics this is repeated for operating each point.

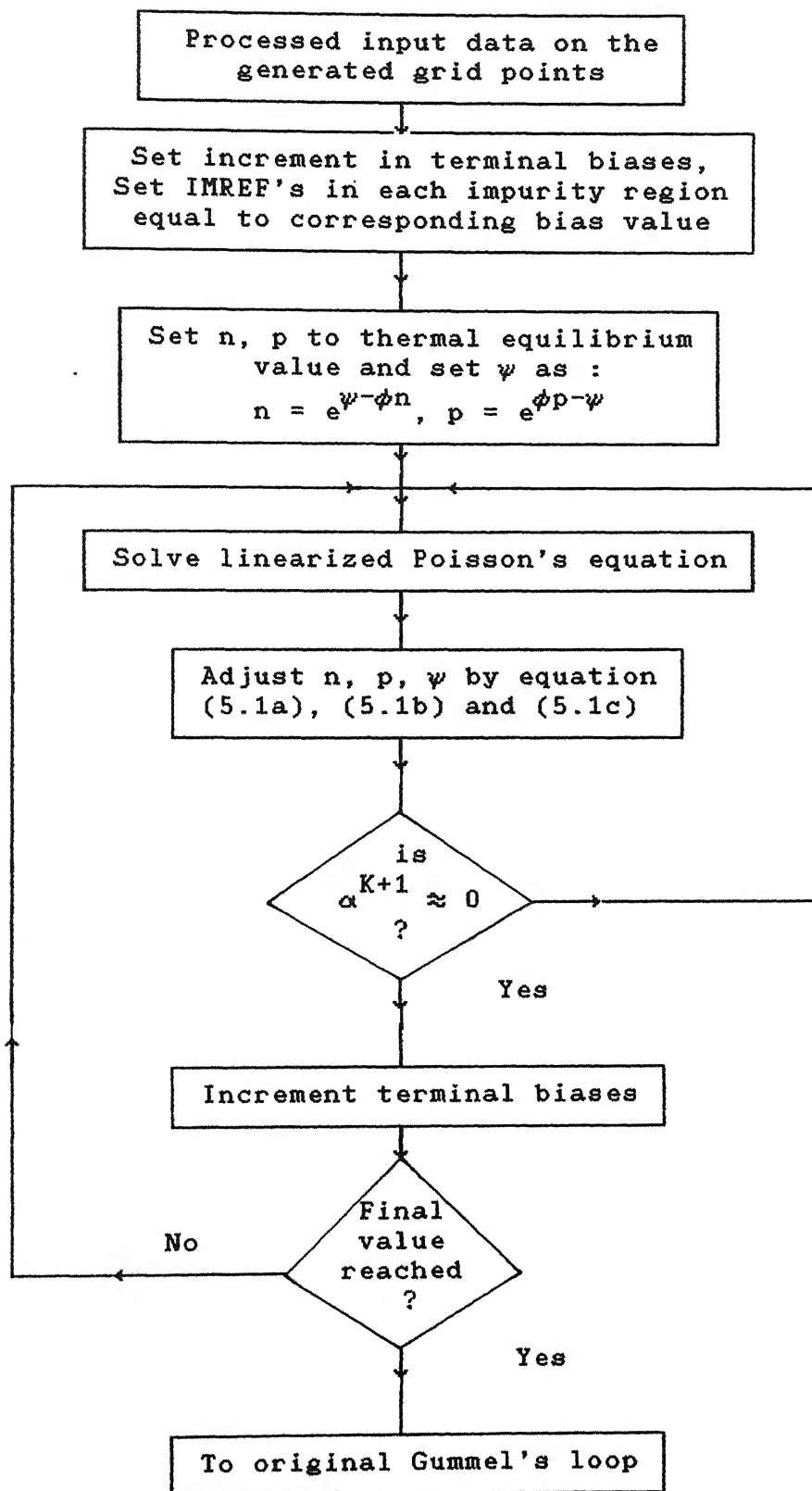


Figure 5.1 : Flow Chart for Initial Guess

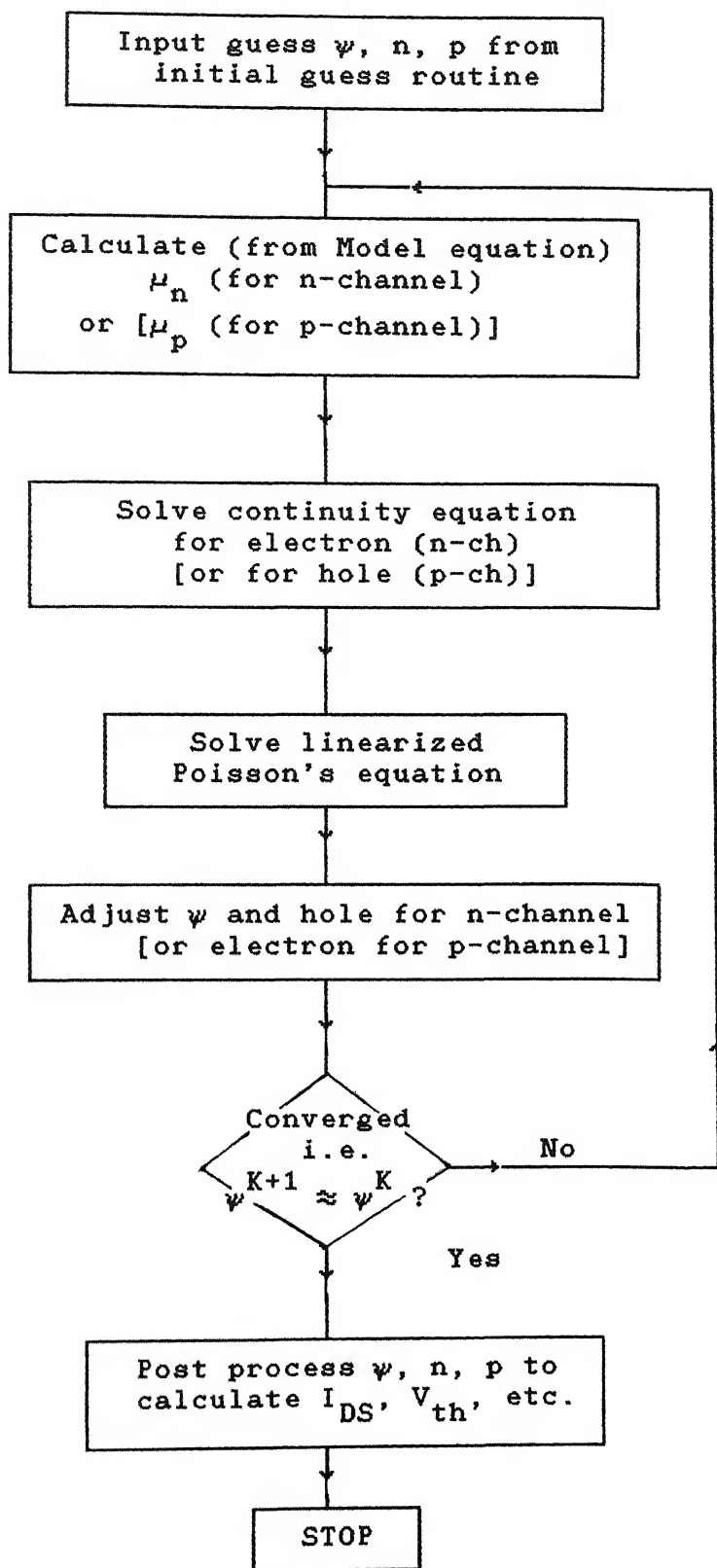


Figure 5.2 : Flow Chart for Gummel's Algorithm

5.2 SOLUTION OF LARGE SPARSE LINEAR SYSTEMS :-

The discretized (5-point molecule) equations for Poisson's and continuity equations are rearranged for computer implementation, with coefficients in the form of ratio of grid spacings, which is necessary to minimize the floating point truncation error during matrix inversion. They look like the following :-

Poisson's equation :

$$\begin{aligned}
 & \alpha_{i,j-1} \left(\frac{h_i + h_{i-1}}{m_{j-1}} \right) + \alpha_{i-1,j} \left(\frac{m_j + m_{j-1}}{h_i} \right) - \alpha_{i,j} \left\{ (m_j + m_{j-1}) \left(\frac{1}{h_i} + \frac{1}{h_{i-1}} \right) \right. \\
 & \quad \left. + (h_i + h_{i-1}) \left(\frac{1}{m_j} + \frac{1}{m_{j-1}} \right) + \frac{(m_j + m_{j-1})}{2} \left(\frac{1}{h_i} + \frac{1}{h_{i-1}} \right) (m_{i,j} + p_{i,j}) \right\} \\
 & \quad + \alpha_{i+1,j} \left(\frac{m_j + m_{j-1}}{h_i} \right) + \alpha_{i,j+1} \left(\frac{h_i + h_{i-1}}{m_j} \right) \\
 & = \frac{(m_j + m_{j-1})(h_i + h_{i-1})}{2} (n_{i,j} - p_{i,j} - C_{i,j}) \\
 & \quad - \left[\psi_{i,j-1} \left(\frac{h_i + h_{i-1}}{m_j} \right) + \psi_{i-1,j} \left(\frac{m_j + m_{j-1}}{h_i} \right) - \psi_{i,j} \left\{ (m_j + m_{j-1}) \left(\frac{1}{h_i} + \frac{1}{h_{i-1}} \right) \right. \right. \\
 & \quad \left. \left. + (h_i + h_{i-1}) \left(\frac{1}{m_j} + \frac{1}{m_{j-1}} \right) \right\} + \psi_{i+1,j} \left(\frac{m_j + m_{j-1}}{h_i} \right) + \alpha_{i,j+1} \left(\frac{h_i + h_{i-1}}{m_j} \right) \right]
 \end{aligned}
 \tag{5.2a}$$

Electron Continuity equation,

$$\begin{aligned}
& n_{i,j-1} \gamma_{n_{i,j-1/2}} B(\psi_{i,j-1} - \psi_{i,j})^{\frac{h_{i-1} + h_i}{m_{j-1}}} \\
& + n_{i-1,j} \gamma_{n_{i-1/2,j}} B(\psi_{i-1,j} - \psi_{i,j})^{\frac{m_j + m_{j-1}}{h_{i-1}}} \\
& - n_{i,j} \left\{ \gamma_{n_{i,j-1/2}} B(\psi_{i,j} - \psi_{i,j-1})^{\frac{h_i + h_{i-1}}{m_{j-1}}} \right. \\
& + \gamma_{n_{i-1/2,j}} B(\psi_{i,j} - \psi_{i-1,j})^{\frac{m_j + m_{j-1}}{h_{i-1}}} \\
& + \gamma_{n_{i,j+1/2}} B(\psi_{i,j} - \psi_{i+1,j})^{\frac{h_i + h_{i-1}}{m_j}} \left. \right\} \\
& + n_{i+1,j} \gamma_{n_{i+1/2,j}} B(\psi_{i+1,j} - \psi_{i,j})^{\frac{h_i + h_{i-1}}{m_j}} \\
& + n_{i,j+1} \gamma_{n_{i,j+1/2}} B(\psi_{i,j+1} - \psi_{i,j})^{\frac{h_i + h_{i-1}}{m_j}} \\
& = \frac{(h_i + h_{i-1})(m_j + m_{j-1})}{2} R_{i,j} \quad (5.2b)
\end{aligned}$$

Hole continuity equation will look a like so, it is not written here.

The family of equation (5.2) gives rise to a large sparse system of linear system as :

$$[A]_{(NX.NY)(NX.NY)} [T]_{(NX.NY)(1)} = [q]_{(NX.NY).(1)} \quad (5.3)$$

The coefficient Matrix has at most 5 non-zero elements. The direct solution of this system is very costly in terms of computer memory. Iterative schemes are found the most suitable for solution of these semiconductor problems.

The main disadvantage of iterative scheme is their slow

convergence. A relative merits and results of different iterative schemes [point-Jacobi, S.O.R., S.L.O.R., ADI etc.] have been discussed in [42].

As Poisson's equation is solved quite a number of times in the algorithm than the continuity equation, so a fast algorithm is chosen, Stone's strongly implicit procedure (S-I-P).

5.2.a Stone's S-I-P :

Stone's idea [36] was to perturb the original [A] by another matrix [N] of same rank but the norm of [N] is much smaller than that of [A], so as to factorize [A+N] easily and factorized lower [L] and upper [U] triangular matrix gives only non-zero elements corresponding to the non-zero places of the original [A]. Figure 5.3 shows the non-zero diagonals of [A], [L] and [U].

In figure 5.4, solid circles represent the standard 5 point molecule for discretization scheme. To get the effect of [N], perturbation matrix, we include the effect of crossed (X) points. Expanding the (X) points in Taylor series and neglecting higher order terms :

$$T_{i-1,j+1} = -T_{i,j} + T_{i,j+1} + T_{i-1,j} \quad (5.4a)$$

$$T_{i+1,j-1} = -T_{i,j} + T_{i+1,j} + T_{i,j-1} \quad (5.4b)$$

To ensure the effect of perturbation minimum right hand sides of equation 5.4 are multiplied by α ($0 < \alpha < 1$) and added to left hand side and finally incorporated in the left hand side of discrete equation $[A][T] = [q]$, L.H.S. becomes

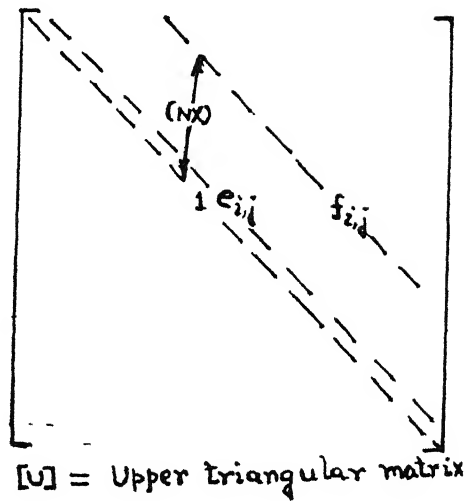
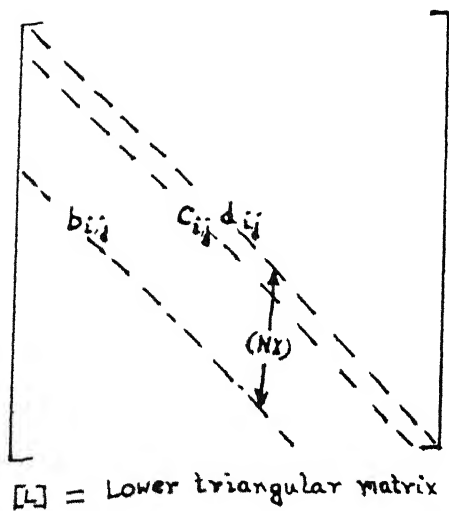
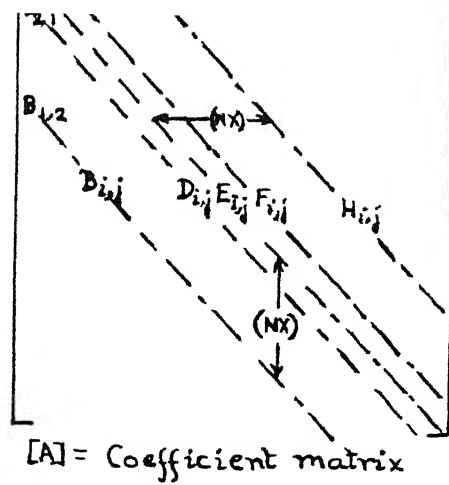


Fig. 5.3
Coefficient matrix $[A]$, lower $[L]$ & upper $[U]$
triangular matrices for Stone's S-I-P

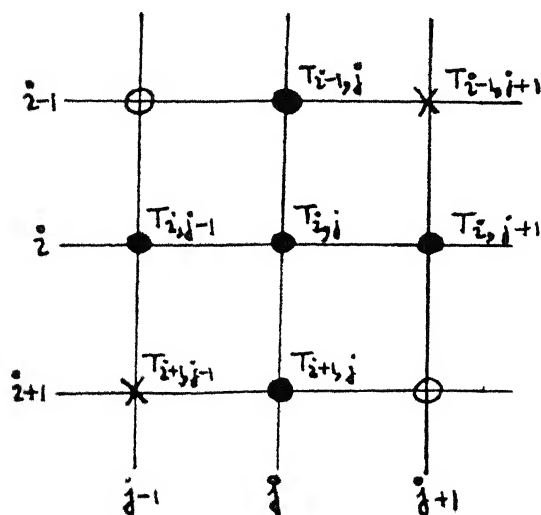


Fig. 5.4
Discretization molecule for the perturbation of
coefficient matrix $[A]$ in Stone's S-I-P

$$\begin{aligned}
& B_{i,j} T_{i,j-1} + D_{i,j} T_{i-1,j} + E_{i,j} T_{i,j} + F_{i,j} T_{i+1,j} + H_{i,j} T_{i,j+1} \\
& + C_{i,j} [T_{i+1,j-1} - \alpha(-T_{i,j} + T_{i+1,j} + T_{i,j-1})] \\
& + G_{i,j} [T_{i-1,j+1} - \alpha(-T_{i,j} + T_{i,j+1} + T_{i-1,j})] \quad (5.5)
\end{aligned}$$

Coefficient $B_{i,j}$ through $H_{i,j}$ are as shown in figure 5.3.

The coefficient matrix now becomes

$$[A'] = [A + N] = [L][U] \quad (5.6)$$

Collecting the terms in equation 5.5 and comparing with the R.H.S. of equation 5.6, we get

$$\left. \begin{aligned} C_{i,j} &= b_{i,j} e_{i,j-1} \\ G_{i,j} &= c_{i,j} f_{i-1,j} \end{aligned} \right\} \quad (5.7a)$$

The terms multiplying them are partially canceled dependent variable at $(i-1, j+1)$ and $(i+1, j-1)$.

The relation obtained relating coefficient of $[A+N]$ and $[L] \times [U]$ are

$$\begin{aligned}
b_{i,j} &= B_{i,j} - \alpha C_{i,j} \\
c_{i,j} &= D_{i,j} - \alpha G_{i,j} \\
d_{i,j} + b_{i,j} f_{i,j-1} + C_{i,j} e_{i-1,j} &= I_{i,j} + \alpha C_{i,j} + \alpha G_{i,j} \\
d_{i,j} e_{i,j} &= F_{i,j} - \alpha C_{i,j} \\
d_{i,j} f_{i,j} &= H_{i,j} - \alpha G_{i,j} \quad (5.7b)
\end{aligned}$$

where, the lower case letters denote the coefficients of $[L]$ and $[U]$ and capital letters for $[A+N]$, as shown in figure 5.3.

From equation 5.3 we can write

$$[A+N][T] = [A+N][T] - ([A][T] - [q]) \quad (5.8a)$$

It gives the iterative scheme equation 5.8b

$$[A+N][T]^{K+1} = [A+N][T]^K - ([A][T]^K - [q]) \quad (5.8b)$$

At any iteration step, coefficient of [L] and [U], i.e., b, c, d, e, f are calculated using the equation family (5.7) by elimination method and equation (5.8b) is solved by LU factorization, until convergence occurs.

The parameter α , called iteration parameter, is chosen optimally. The range of α is [0, 1]. But two small value of α causes convergence problem. A set of α values ranging from 0.6 to 1.0 is tried; a value around $\alpha = 0.98$ is found suitable for faster convergence of S-I-P.

5.2.b Successive Line Relaxation :

Continuity equation yields a coefficient matrix which is rather ill conditioned. It has been found very difficult to solve continuity equation by S-I-P. So, this successive line relaxation iterative technique is used here.

It is based on a sequential update of the solution according to the block of nodes [37]. For these techniques unknown vector [T] is divided into NX blocks corresponding to the horizontal lines of a grid structure (figure 4.1). The elements of [A],[T],[q] becomes blocks of matrices as $[B]_i$, $[C]_i$, $[D]_i$, $[T]_i$, and $[q]_i$ for the i^{th} X-line on the grid (figure 4.1), and [A]

becomes block tridiagonal matrix [37], as

$$[A] = \begin{bmatrix} C_1 & & & & \\ B_2 & D_1 & & & \\ & B_i & C_i & D_i & \\ & & B_{NX} & C_{NX} & \end{bmatrix}$$

The diagonal blocks $[C_i]$ are again tri-diagonal and $[B]_i$ and $[D]_i$ are only diagonal matrices.

It is solve by the iterative scheme as :-

$$[T]_i^{K+1} = (1-w)[T]_i^K + w[C]_i^{-1} \left\{ [q]_i - [B]_i [T]_{i-1}^K - [D]_i [T]_{i+1}^K \right\} \quad (5.9)$$

for $i = 1$ to NX

Where, the relaxation parameter, w , is in the range $0 < w < 2$ [37], [38].

As done in case of α , value of w is set to 1.2.

This type of iterative scheme requires low amount memory and they are very easy to program.

5.3 POST-PROCESSING OF ψ , n , p :-

We get ψ , n , p as solution of semiconductor equation by Gummel's algorithm; now we extract I_{DS} , V_{th} from the results obtained.

5.3.a Current Calculation :

Pao and Sah's model [40] was developed long ago to calculate

current in MOS, excluding the effect of source and drain junctions and taking one dimensional Poisson's equation in the channel. This model is modified by De la Moneda [19], is used here.

Assuming predominant current flow in lateral direction, for electron, it is re-written as

$$J_{ny} = \gamma_n e^{\psi} \frac{\partial e^{-\phi_n}}{\partial y} \quad (5.10)$$

Neglecting recombination generation current, and integrating the differential element [figure 5.5] $J_{ny} dx d\chi$ over X-Z plane, we get

$$I_{DS} = W \left[\frac{de^{-\phi_n}}{dy} \right] \int_0^d \gamma_n e^{\psi} d\chi \quad (5.11a)$$

where d and W are defined in the figure 5.5.

$$\text{Defining } F(\chi) = \int_0^d \gamma_n e^{\psi} d\chi \quad (5.11b)$$

and carrying out an additional integration over channel length L we get current expression :

$$I_{DS} = W \frac{e^{-\phi_n(0)} - e^{-\phi_n(L)}}{\int_0^L F(\chi)^{-1} d\chi} \quad (5.11c)$$

where $x = 0$: source contact edge near gate

$x = L$: drain contact edge near gate

Similar is the current relation for p-channel MOS.

5.3.b Threshold Voltage (V_{th}) :-

V_{th} , for simulation and practical problems, is the gate voltage at which the device sinks $0.1 \mu A \times (W/L)$ amount of current [41]. Usually V_{th} is calculated for $V_{DS} = 0.2 V$ or any value close to it. at higher V_{DS} , V_{th} decreases due to drain induced barrier lowering [18].

One scheme, derived from the subthreshold current expression of MOS, which varies exponentially with V_{GS} , states [14]

$$V_{th}^j = V_{th}^{j-1} + \ln \left\{ \frac{I_{th}}{I_D^{j-1}} \right\} \left\{ \frac{\Delta \ln (I_D/I_{th})}{\Delta V_G} \right\}^{-1} \quad (5.12)$$

where, superscripts are the values at j -th iteration of the Newton-Rapson scheme given in equation 5.12.

$$I_{th} = 0.1 (W/L) \mu A$$

V_{th}^0 = starting guess for V_{th} (V_{th}^0 may be from long channel V_{th} formula obtained in any text [10])

$$I_D^{j-1} = \text{drain current at } V_G = V_{th}^{j-1}$$

The derivative is calculated by giving increment on $V_G = V_{th}^{j-1} + \Delta V$ ($\approx 50 \text{ mV}$).

The stopping criterion for convergence is set

$$\left| V_{th}^j - V_{th}^{j-1} \right| \leq 1 \text{ mV.}$$

5.4 CONVERGENCE CRITERION OF GUMMEL'S ALGORITHM USED :-

Figure 5.6 shows the convergence criterion of the iterative algorithm. The normalized error is the root mean square error in potential at i -th iteration. Iteration counts are the iteration number of the Gummel's algorithm and counting starts after the initial guess loop ends [figure 5.1]. It is found that 10 to 35 iterations through Poisson's equation solution and p-n adjustment and bias increments are needed for a good initial guess; the number depends on bias values and number of grids.

It is found in figure 5.6, when the MOS not in strong inversion ($V_G = 0.5V$, $V_D = 3V$) only 7 Gummel's iterations are needed for convergence. But under strong inversion ($V_G = 3V$ and $V_D = 3V$:same) convergence is slower, takes 60 iterations. This is due to strong coupling between Poisson's and continuity equations.

It is also noted that, in this simulation, initial guess iteration plus Gummel's iteration is within 100, owing to the better initial guess in this simulation.

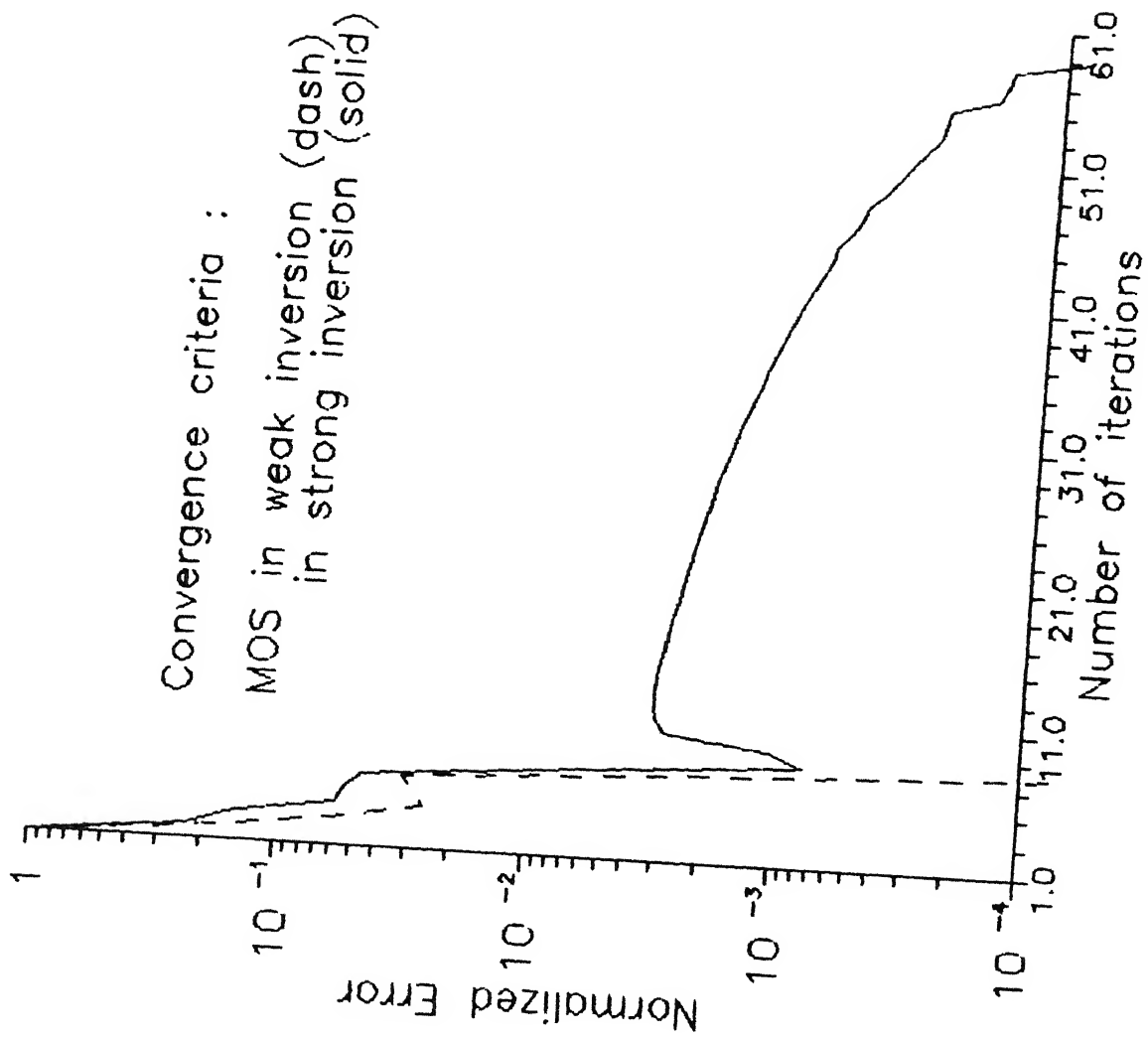


Fig. 5.6
Convergence criteria of Gummel's algorithm

Chapter 6

SIMULATED EXAMPLES

It is rather difficult to present all the possible simulation results here. Examples are chosen which cover some of the problems and remedies associated with the miniaturized MOSFETs . The examples are simulated with the help of the two dimensional simulation program developed .

6.1 SIMULATED DEVICES :-

In this series of examples the devices chosen are the short channel MOSFETs with no implantation in the channel (DEVICE 1), with one shallow channel implantation (DEVICE 2) and with two channel implantations (DEVICE 3) .

6.1a. DEVICE 1 :

Figure 6.1a shows the input file [explained in the appendix] of the DEVICE 1, n-channel MOSFET. The gate mask length (l) is 1.5 μm , width (w) is 10 μm , oxide thickness (t_{ox}) of 500 Å, source and drain contact lengths (upto which simulation is done), are 0.3 μm . Source and drain are implanted with a Phosphorus- dose of 10^{15} atoms/ cm^2 , range (rp) and straggle (drp) are set so that junction depth be approximately 0.3 μm ; the substrate concentration (subs)


```

title    DEVICE-1
device   type='n', sd=0.3e-4, l=1.50e-4, w=10.e-4,
+        tox=500.e-8, d=2.5e-4
bias     ud=3.0, ug=0.0, us=0.0, ub=0.0, vfb=-0.8
comnt    No channel implantation
profile  subs=-1.e15, dose=1.00e15, rp=0.0, drp=6.01e-6
comnt    Distribution of potential, n, p & doping profile
option   model='distrib'
end

title    DEVICE-2
device   type='n', sd=0.3e-4, l=1.50e-4, w=10.e-4,
+        tox=500.e-8, d=2.5e-4
bias     ud=3.0, ug=0.0, us=0.0, ub=0.0, vfb=-0.8
comnt    one shallow channel implantation
profile  subs=-1.e15, dose=1.00e15, rp=0.0, drp=6.01e-6
+        dosec1=-3.e11, rpc1=0.0, drpc1=6.e-6
comnt    Distribution of potential, n, p & doping profile
option   model='distrib'
end

title    DEVICE-3
device   type='n', sd=0.3e-4, l=1.50e-4, w=10.e-4,
+        tox=500.e-8, d=2.5e-4
bias     ud=3.0, ug=0.0, us=0.0, ub=0.0, vfb=-0.8
comnt    two channel implantations
profile  subs=-1.e15, dose=1.00e15, rp=0.0, drp=6.01e-6
+        dosec1=-3.e11, rpc1=0.0, drpc1=6.e-6
+        dosec2=-2.e11, rpc2=3.9e-5, drpc2=8.e-6
comnt    Distribution of potential, n, p & doping profile
option   model='distrib'
end

```

Fig. 6.1

Input files for (a) DEVICE 1, (b) DEVICE 2 &
(c) DEVICE 3

is 10^{15} /cc of p-type impurity (Boron) .The device is biased at :
 $u_s=u_b=0$ v, $u_g= 0$ v, $u_d= 3$ v, flatband voltage is set to -0.8 v (only taking work function difference of Si and gate metal Al).

From the quasi 3-dimensional plot of the doping profile set by the program (fig.6.2a, source on the left) source - drain peak concentration is measured to be slightly less than 10^{20} /cc (value given in the output file is $0.6655E20$ /cc).The output file records vertical junction depth (x_j) equal to $0.28\mu\text{m}$ and lateral spread is approximately the same. So the metallurgical channel length is reduced to $0.94\mu\text{m}$.

Figure 6.2b shows the quasi three dimensional and figure 6.2c shows the contour plots of the potential distribution within this DEVICE 1 . The potential at source and drain contacts are found to be higher than what is applied by 0.8 v, which is built in potential of the junctions. In the depletion region of the reverse biased drain-bulk junction, it decreases monotonically, and it is nearly constant in the highly doped source & drain regions . It is clear from the source-channel potential variation that there is hardly any barrier. So this device is on even at zero gate voltage.

The above feature is very clear from the electron distribution (fig. 6.2d) . The surface concentration of electrons in the channel is high enough ($\cong 6 \times 10^{15}$ /cc, above the substrate concentration) to cause inversion in the channel . It is also to be noted that surface concentration of electron decreases near drain end; it explains the occurrence of pinch-off in the channel.

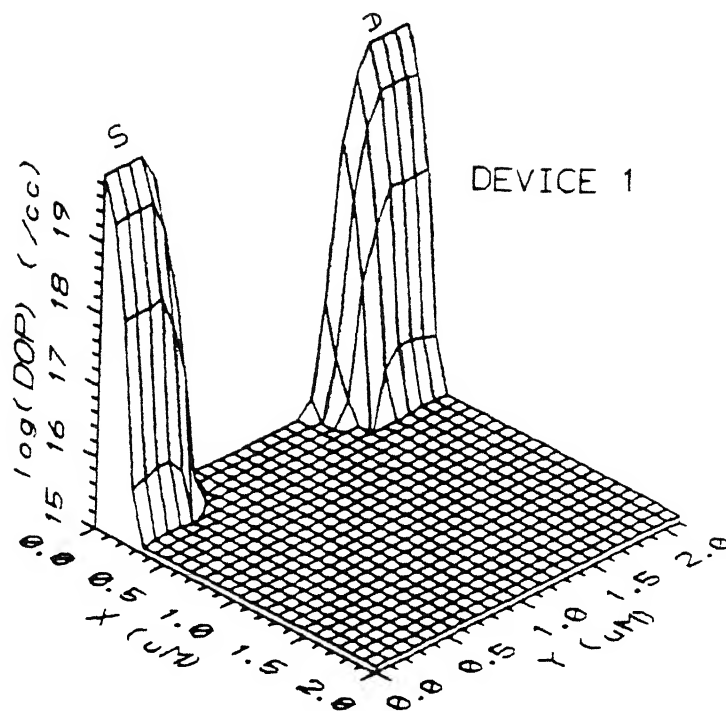


Fig. 6.2a
Doping profile of DEVICE 1

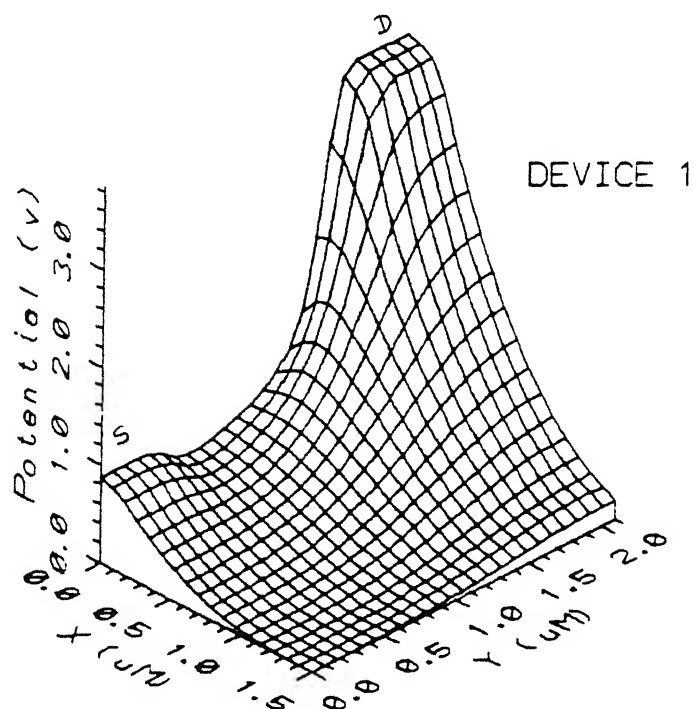


Fig. 6.2b
Potential distribution of DEVICE 1 [$u_g=0v$, $u_d=3v$]

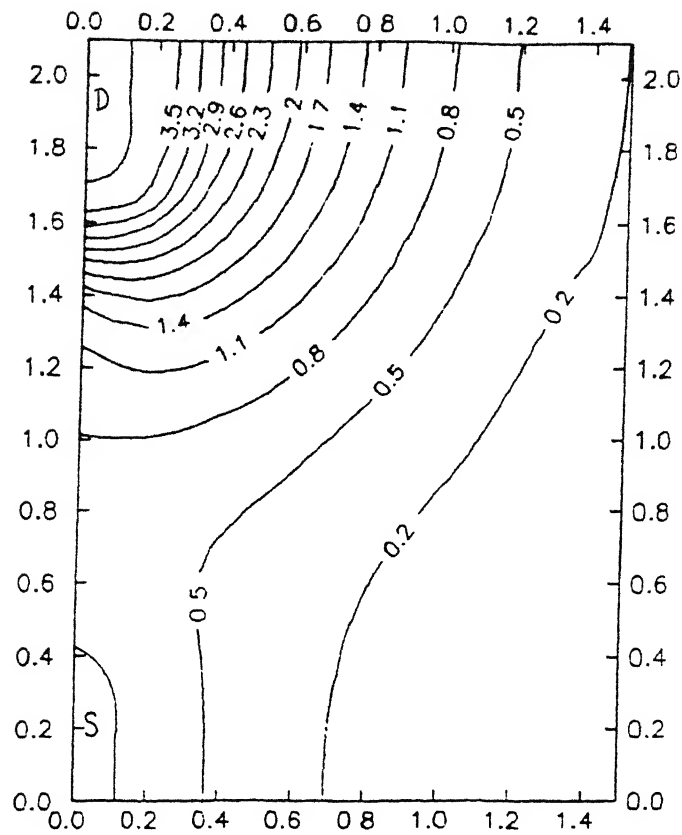


Fig. 6.2c
Isopotential contours of DEVICE 1 [$u_g=0v$, $u_d=3v$]

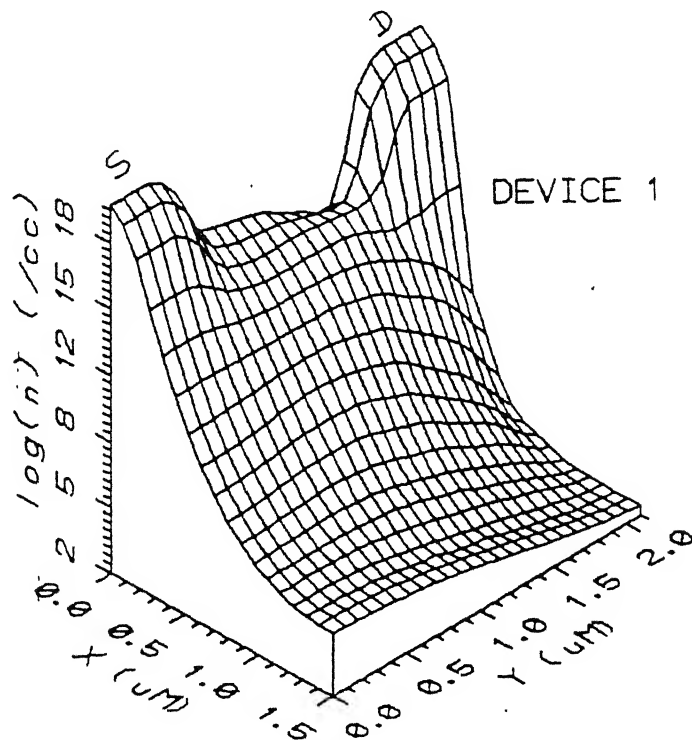


Fig. 6.2d
Concentration of electron of DEVICE 1 [$u_g=0v$, $u_d=3v$]

One more thing very clear from fig 6.2d, is that, there is an unexpected bulge of electron concentration at a depth of about 0.5 to 0.6 μm . This is the proof of "punch-through" present at the said drain voltage, the bulge of electron supports the punch-through current flowing away from the surface. The punch-through is further supported by the merge of drain and source depletion regions in the figure 6.2c. This punch-through and unexpected formation of inversion layer (i.e., decrease of threshold voltage) are the major problems of short channel MOS.

6.1b. DEVICE 2 :

The input file of this device is shown in figure 6.1b. All other conditions are same as DEVICE 1 except, there is a shallow p-type channel implant to increase the threshold voltage, i.e., to make DEVICE 2 normally off.

From the impurity distribution (fig. 6.3a) peak concentration and the depth of the channel implant are measured to be $2 \times 10^{16}/\text{cc}$ and 0.257 μm respectively. This high concentration inhibits formation of inversion layer.

Figure 6.3b and 6.3c show the quasi 3-d and contour plots of the potential distribution in DEVICE 2, under same bias as before. The quasi 3-d plot looks like that of DEVICE 1, but the contour plots show there is slight barrier formation in source - channel compared to DEVICE 1. It also shows that the single channel implantation is unable to separate the depletion regions of the

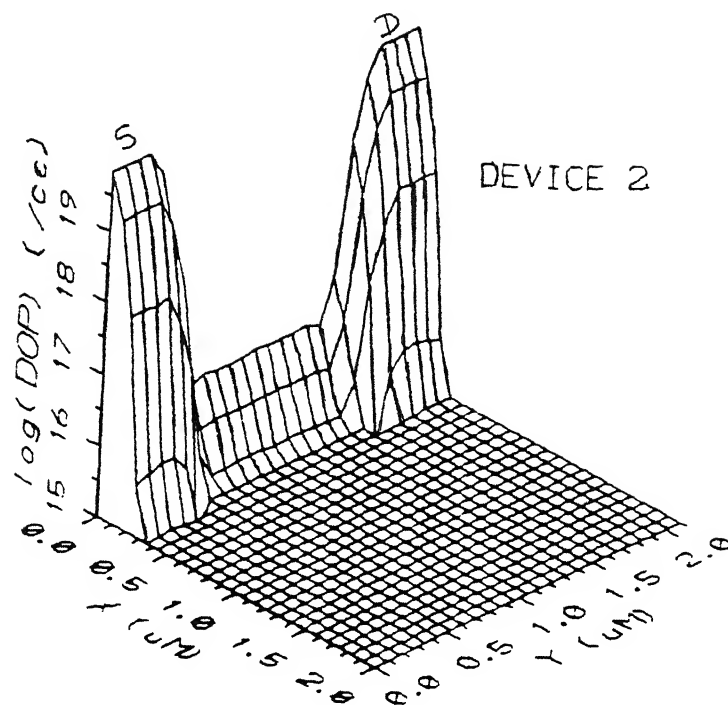


Fig. 6.3a
Doping profile of DEVICE 2

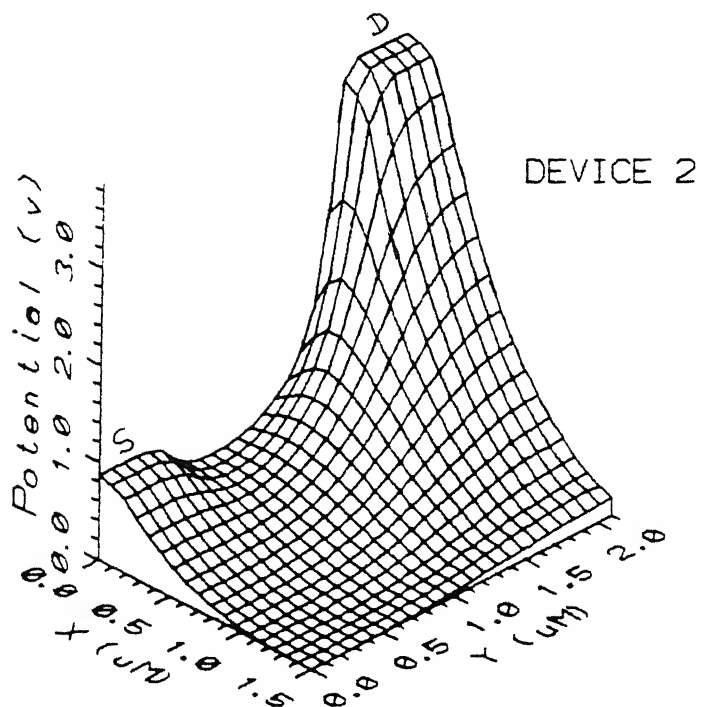


Fig. 6.3b
Potential distribution of DEVICE 2 [$u_g=0v$, $u_d=3v$]

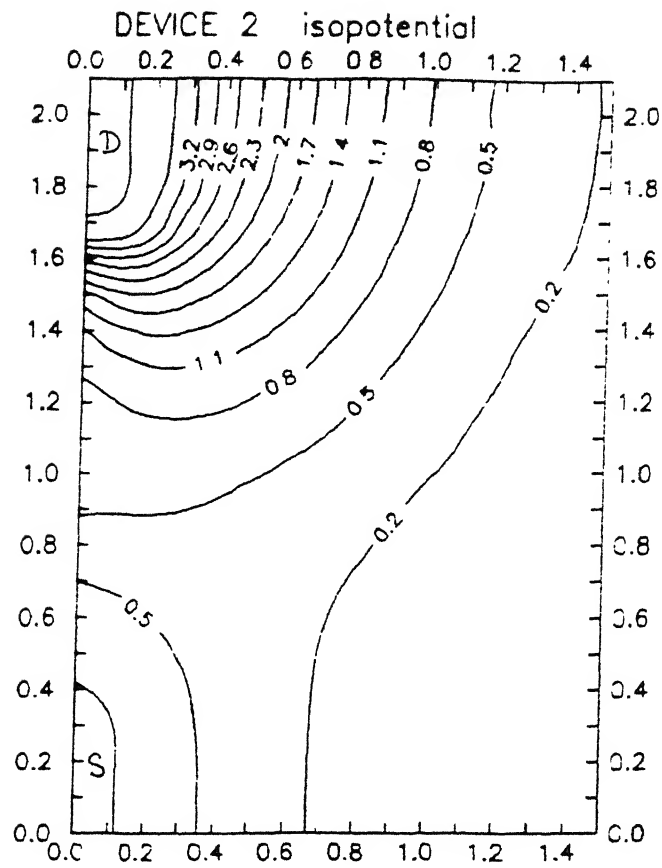


Fig. 6.3c
Isopotential contours of DEVICE 2 [$u_g=0v$, $u_d=3v$]

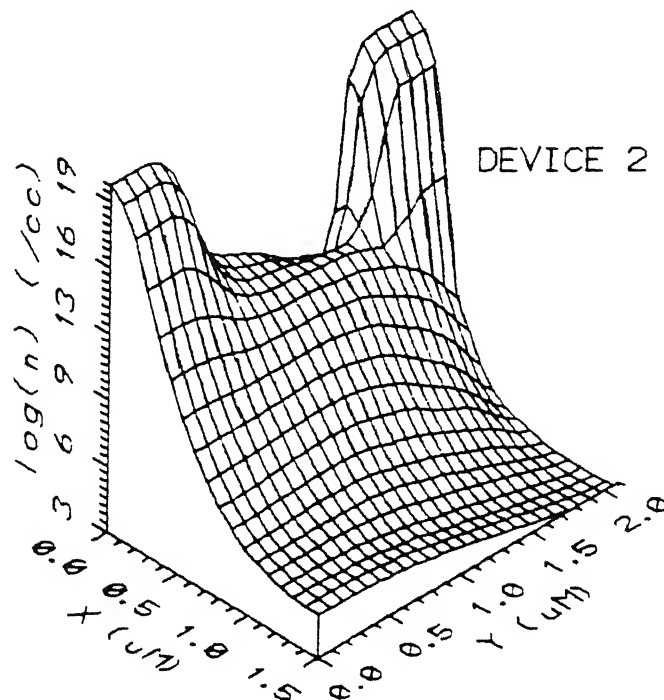


Fig. 6.3d
Concentration of electron of DEVICE 2 [$u_g=0v$, $u_d=3v$]

DEVICE 2 (back)

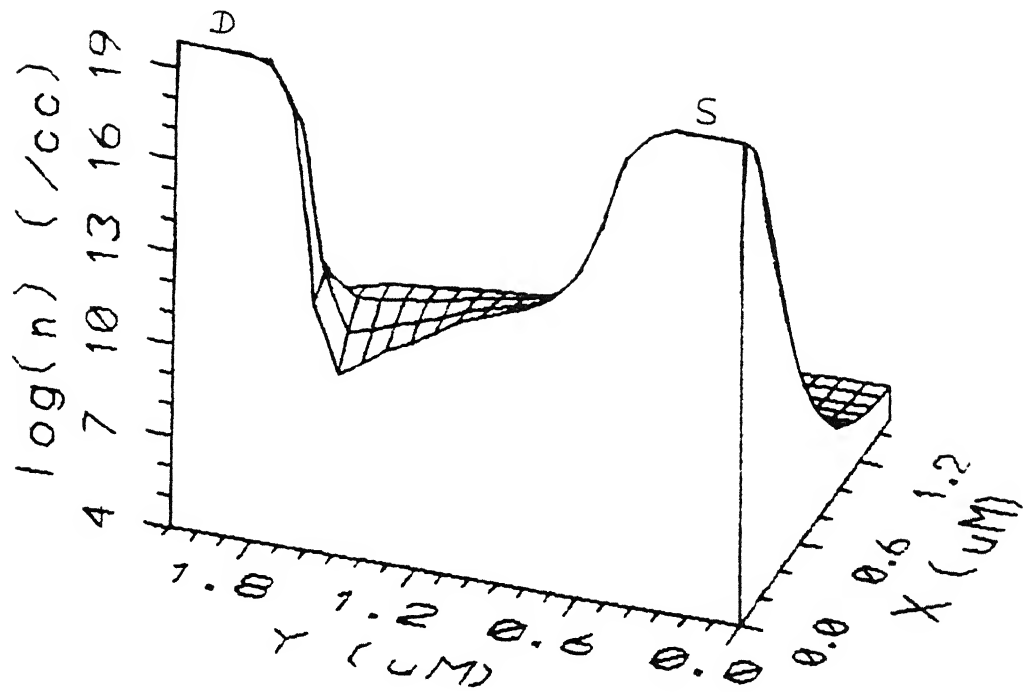


Fig. 6.3e

Concentration of electron of DEVICE 2 [$u_g=0\text{v}$, $u_d=3\text{v}$], looking through the gate (back side of Fig. 6.3d)

source and the drain. So punch-through occurs here. This is further supported by the similar bulge of electron concentration away from the surface (fig. 6.3d) .

The surface concentration of electrons has decreased to the value $1.2 \times 10^{14}/\text{cc}$ (less than surface acceptor concentration) as expected by the channel implant, no inversion occurs at $u_g=0\text{v}$. So one of the short channel problem has vanished, but there is still the problem of punch-through.

Figure 6.3e is the quasi 3-d plot of electrons looking through the gate . It exaggerates the pinch-off of the channel. Near drain, the surface electron concentration sharply decreases at the surface but it increases at a slight depth from the surface. So, in the pinch - off region, current flows away from the surface and comes back to the drain contact. Hence we need 2-dimensional simulation to track this phenomenon .

6.1c. DEVICE 3 :

As shown in figure 6.1c, DEVICE 3 has one more p-type deep implantation, which we will see controls punch-through, while other input conditions are same as that of DEVICE 2. The concentration profile (fig. 6.4a) gives the peak concentration of the second implant is $1.07 \times 10^{16}/\text{cc}$ occurs near a depth of $0.4\mu\text{m}$ and spreads upto $0.6\mu\text{m}$ inside the bulk. It can be seen from the figure 6.4b that there is a source channel potential barrier at the source end. Two distinct depletion regions, for source and

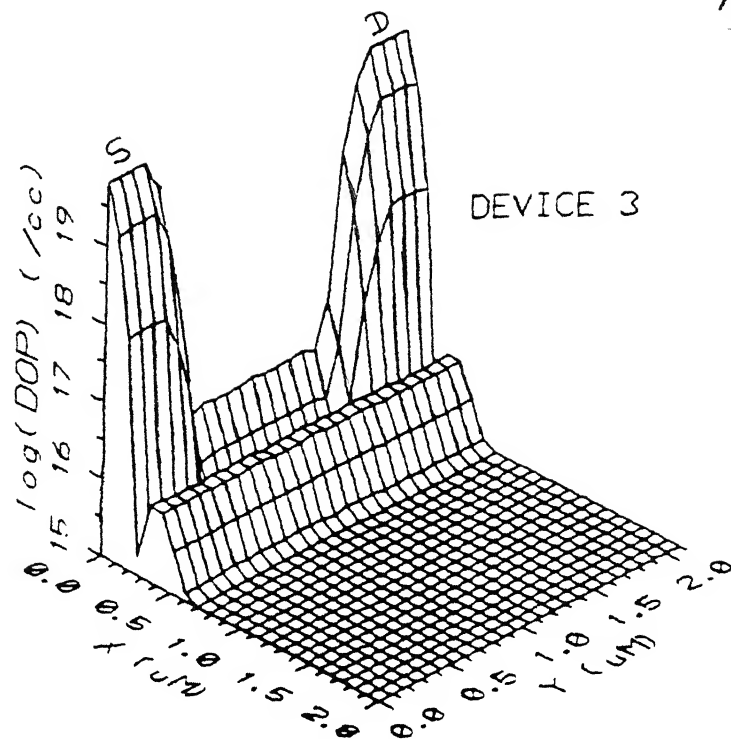


Fig. 6.4a
Doping profile of DEVICE 3

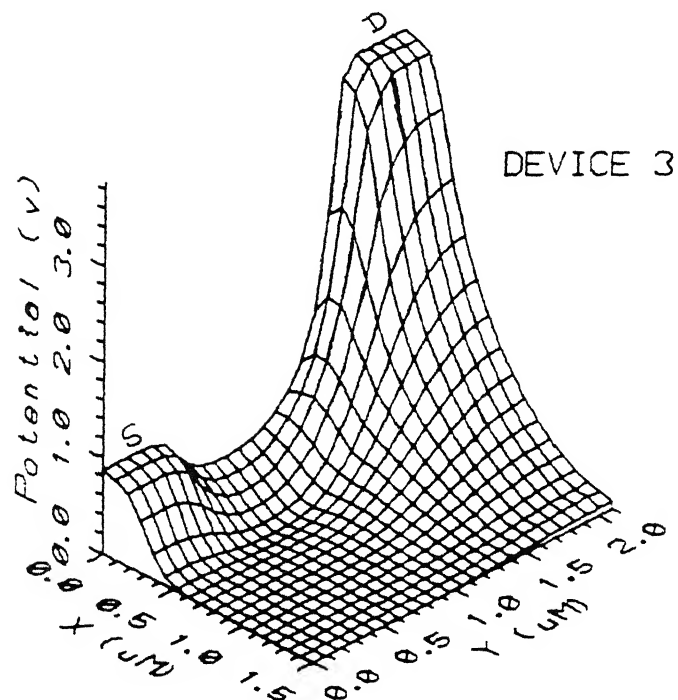


Fig. 6.4b
Potential distribution of DEVICE 3 [$u_g=0v$, $u_d=3v$]

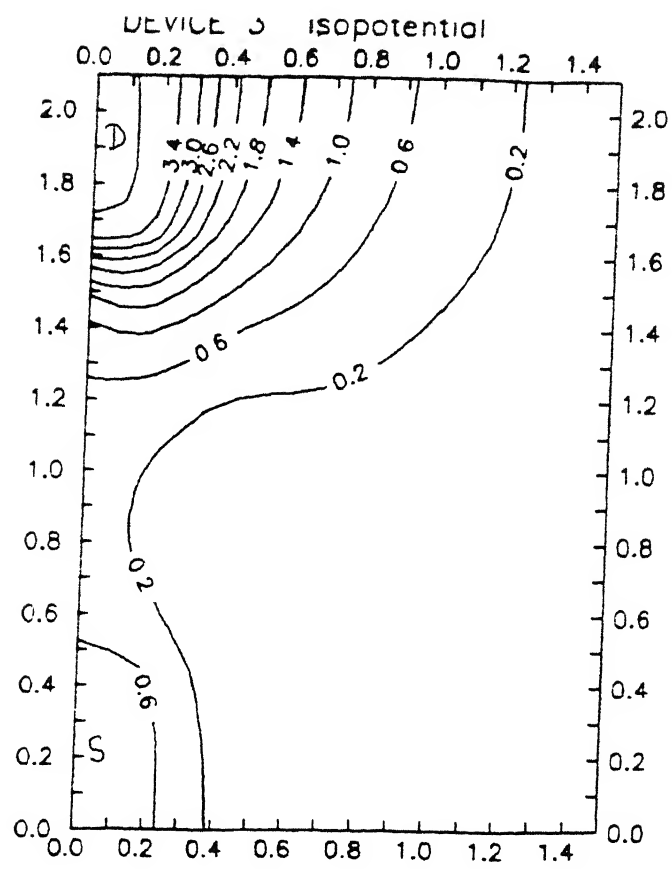


Fig. 6.4c
Isopotential contours of DEVICE 3 [$u_g=0v$, $u_d=3v$]

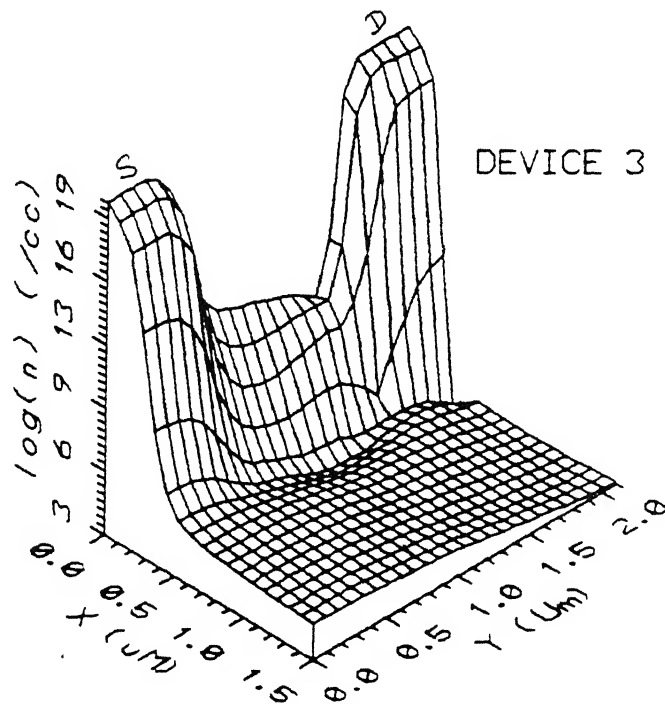


Fig. 6.4d
Concentration of electron of DEVICE 3 [$u_g=0v$, $u_d=3v$]

DEVICE 3 (strong inversion)

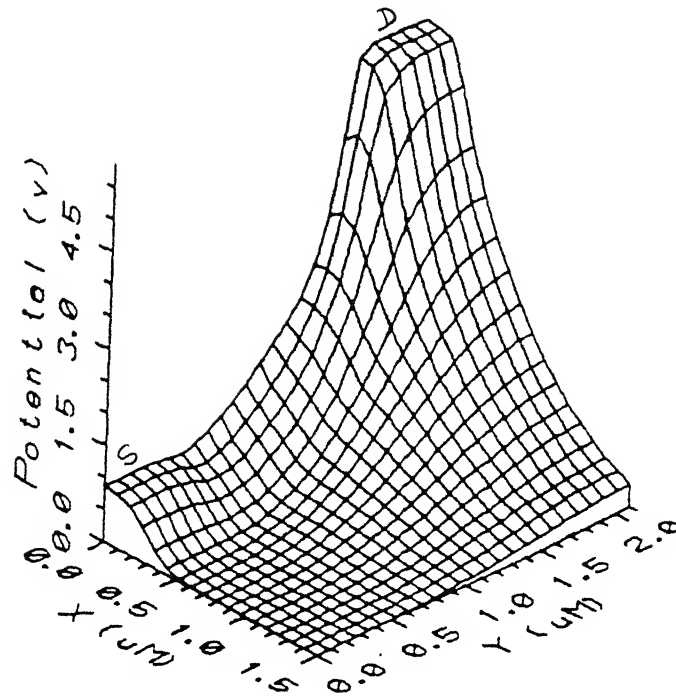


Fig. 6.4e
Potential distribution of DEVICE 3 under strong inversion [$u_g=2v$, $u_d=5v$]

DEVICE 3 (strong inversion)

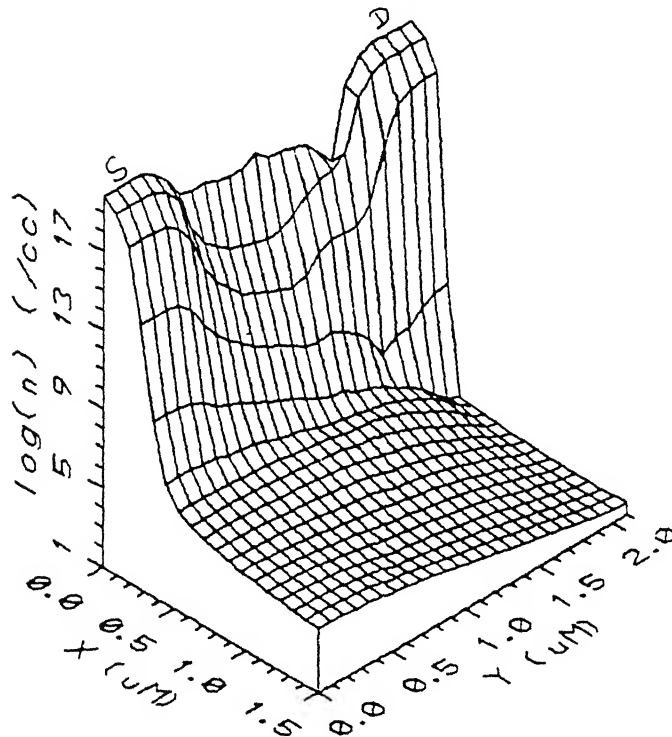


Fig. 6.4f
Concentration of electrons of device 3 under strong

drain, can be noted in the isopotential plot (fig. 6.4c), it explains the clear suppression of the punch-through .

Figure 6.3d is the electron distribution in DEVICE 3. The major difference from the last two devices, is the absence of any bulge of electron concentration away from the surface, this is one more indication for the suppression of punch-through. The surface concentration of electron is less than surface dopant concentration, so no formation of inversion layer at zero gate voltage . Hence we can infer that, two short channel effects, low threshold voltage and punch-through, are overcome in DEVICE 3.

So far, no distribution is shown for MOSFET in strong inversion. Figure 6.4e and figure 6.4f show the potential and the electron concentration distribution under strong inversion (2v at gate) respectively. The concentration of electron at the surface is very high (clear from comparing with fig. 6.4d); the decrease of electron concentration near drain contact shows pinch off as u_d is set at 5v.

6.2 . COMPARISON OF TERMINAL CHARACTERISTICS OF THE THREE DEVICES DESCRIBED :-

So far comparison is made on basis of the distribution of potential and majority carrier concentration of DEVICE 1, DEVICE 2 and DEVICE 3 at a particular operating point . Now comparison will be shown with respect to the simulated terminal characteristics for several operating points .

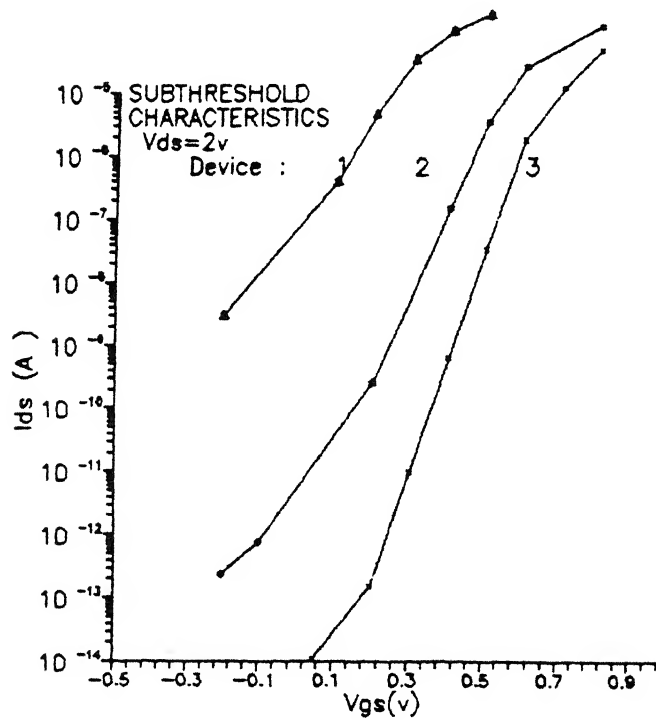
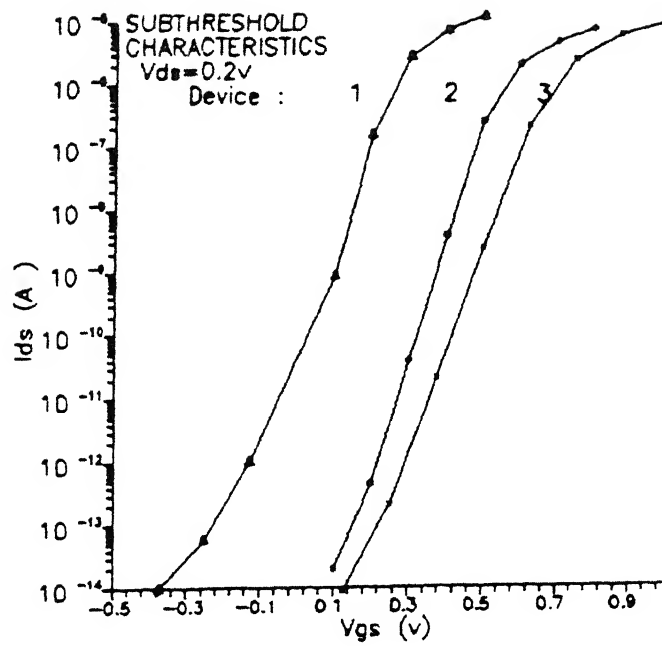


Fig. 6.5
 Subthreshold characteristics of the three devices
 (a) $u_d=0.2\text{ v}$ & (b) $u_d=2.0\text{ v}$

6.2a. Subthreshold characteristics :

It is the drain current vs. gate voltage characteristics below the threshold voltage. The subthreshold region is particularly important in low power and low voltage applications, such as, MOS used as a switch in the digital logic circuits. These characteristics say how the MOS -switch is turned on and off.

Figure 6.5a shows the subthreshold characteristics for the three devices at 0.2v of drain bias (0.2v is chosen as low state logic voltage is around this value). It is clear from the semilog plot that, the drain currents fall off exponentially with gate voltage, which tally with the theory [10]. The slight shift from the linear fall of the semilog plot at very low current below 10^{-13} A is due to the accuracy limitation of the simulation program.

One important parameter extracted from the plot is the *subthreshold swing* (S), defined conventionally as the inverse of the slope of I_{ds} (in \log_{10} scale) vs. gate voltage. S measures how fast the MOS - switch can be turned off and on, the steeper the slope (hence smaller S), the less gate voltage sweep is needed to change state of the switch. For $V_{ds}=0.2v$, S is nearly same for all the three devices, approximately 80-85 mV/decade of I_{ds} ; but the residual I_{ds} increases from DEVICE 3 to DEVICE 1. The drain currents levels off as gate voltage approaches threshold voltage.

When drain voltage increases to 2v (fig. 6.5b), there is no

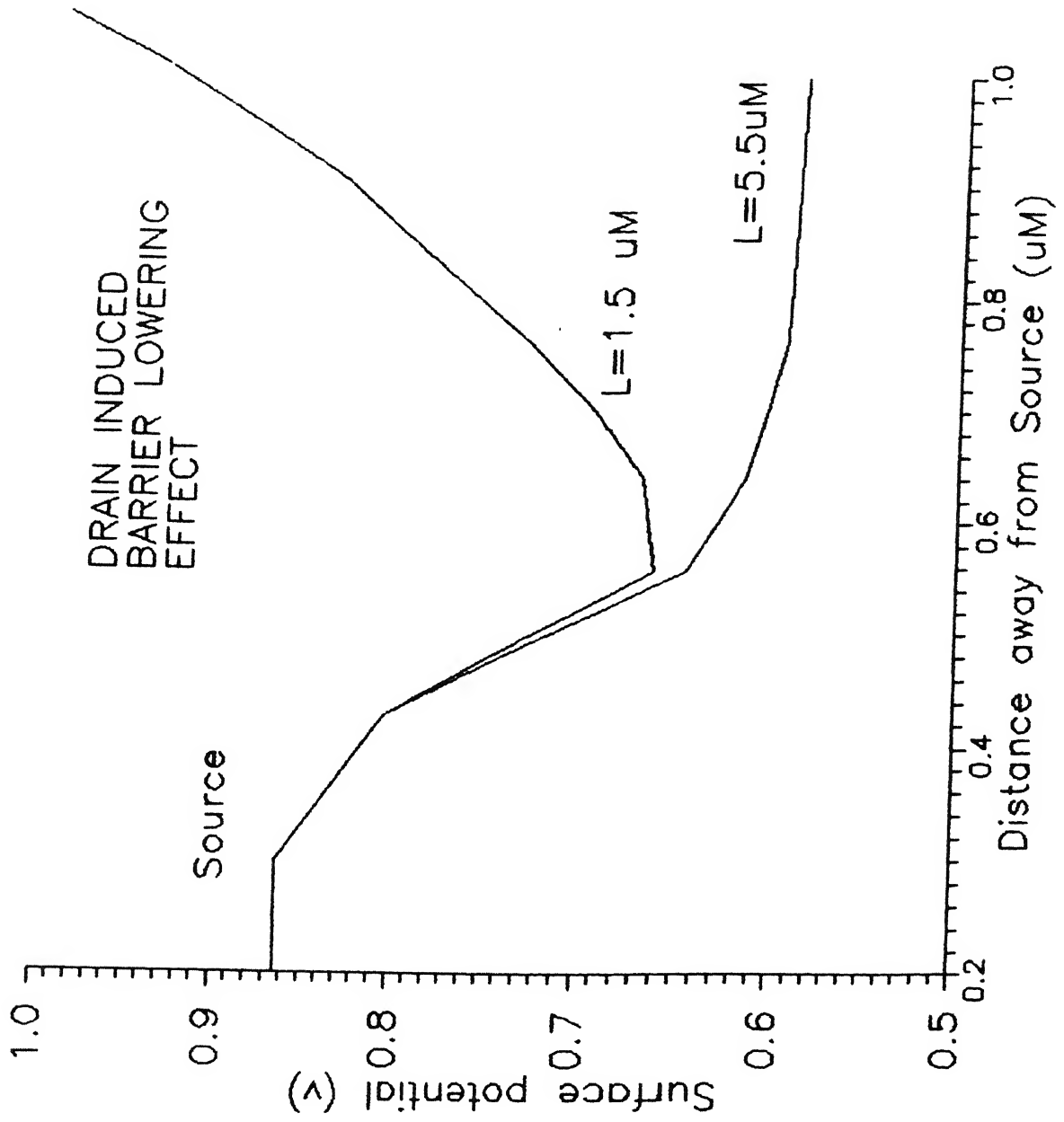


Fig. 6.6
Surface potential distribution along the channel

substantial change of S in case of DEVICE 3, but S increases to 100mV/decade of I_{ds} in case of DEVICE 2 and a drastic change is observed in case of DEVICE 1 ($S = 200\text{mV/decade}$). The residual current increases the maximum in case of DEVICE 1.

The shift of subthreshold characteristics at higher drain voltage is due to the *drain induced barrier lowering* (DIBL) effect [18] for short channel MOSFETs. This is explained in figure 6.6. For long channel ($l=5.5\mu\text{m}$) and for short channel ($l=1.5\mu\text{m}$) n-MOS, the surface potentials near source junction are shown. It is seen that potential barrier between source and channel decreases in case of short channel one (both are biased at $u_g=0$ & $u_d=5\text{v}$). The reason for this barrier lowering is due the proximity of drain and source depletion region in case of short channel MOS. The leakage I_{ds} is exponentially dependent on this barrier.

6.2b. Output characteristics :

The output characteristics of the three devices for a gate bias of 1v are shown in figure 6.7. I_{ds} level decreases from DEVICE 1 to DEVICE 3, because surface electrons (inversion layer) are maximum in the 1st device and decreases by the channel implants in other two devices. The slope of the output characteristics in the saturation region for the DEVICE 1 is large (so λ is large) compared to other two devices; this is one more proof for the pronounced punch-through in DEVICE 1.

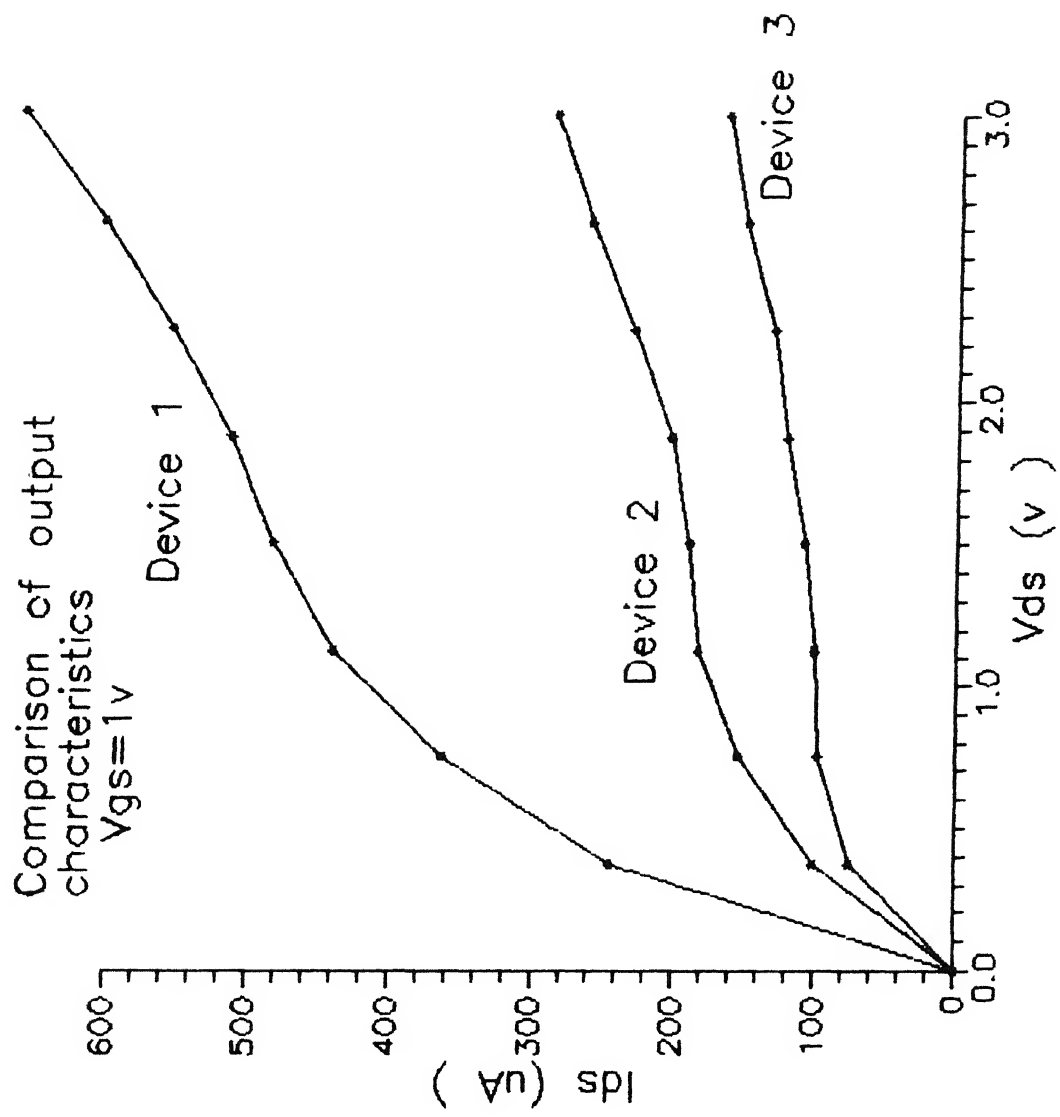


Fig. 6.7
Output characteristics of the three devices for $u_g=1\text{v}$

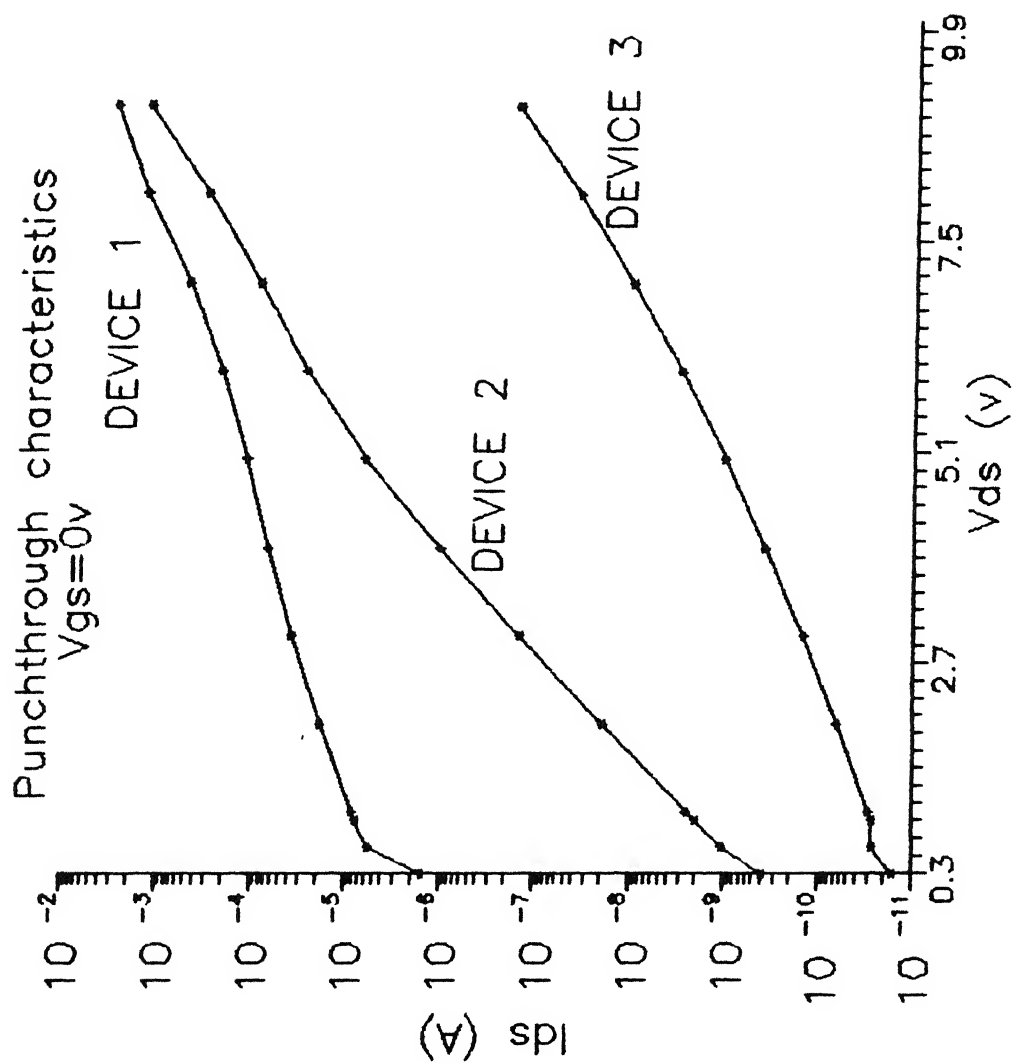


Fig. 6.8
Punch-through characteristics of the three devices
[$u_g=0V$]

6.2c. Punch-through characteristics :

Figure 6.8 shows the semilog plot of the punch-through characteristics of the three devices when gate voltage is zero. This plot shows the drastic increase of I_{ds} for V_{ds} crossing a value, due to the flow of current along the merged depletion regions of source and drain. From these characteristics, punch-through voltage (V_{pt}) can be measured. V_{pt} is defined as the drain voltage at which channel current is equal to a reference value. Different reference values in the range of 10^{-8} to 10^{-9} A are chosen for different applications [18]. Let us choose 10^{-8} A for the channel width of $10\mu\text{m}$. DEVICE 1 is already on even at zero gate voltage, so V_{pt} cannot be measured here. For DEVICE 2 it is found to be 1.4V. This effect of punch-through at low V_{ds} has been observed in sec.6.1b.

For DEVICE 3, V_{pt} is found to be 7.7V. It again proves the effectiveness of the deep channel implant in short channel devices.

6.2c. Threshold voltage :

For the calculation of V_{th} by threshold model, we use 0.2V at drain. Threshold voltage vs. channel length (l) is shown in fig.6.9. It is found that typical short channel effect (fall of V_{th}) starts at a channel length of $2\mu\text{m}$ approximately.

DEVICE 1 is found normally on as its V_{th} is -0.006V for

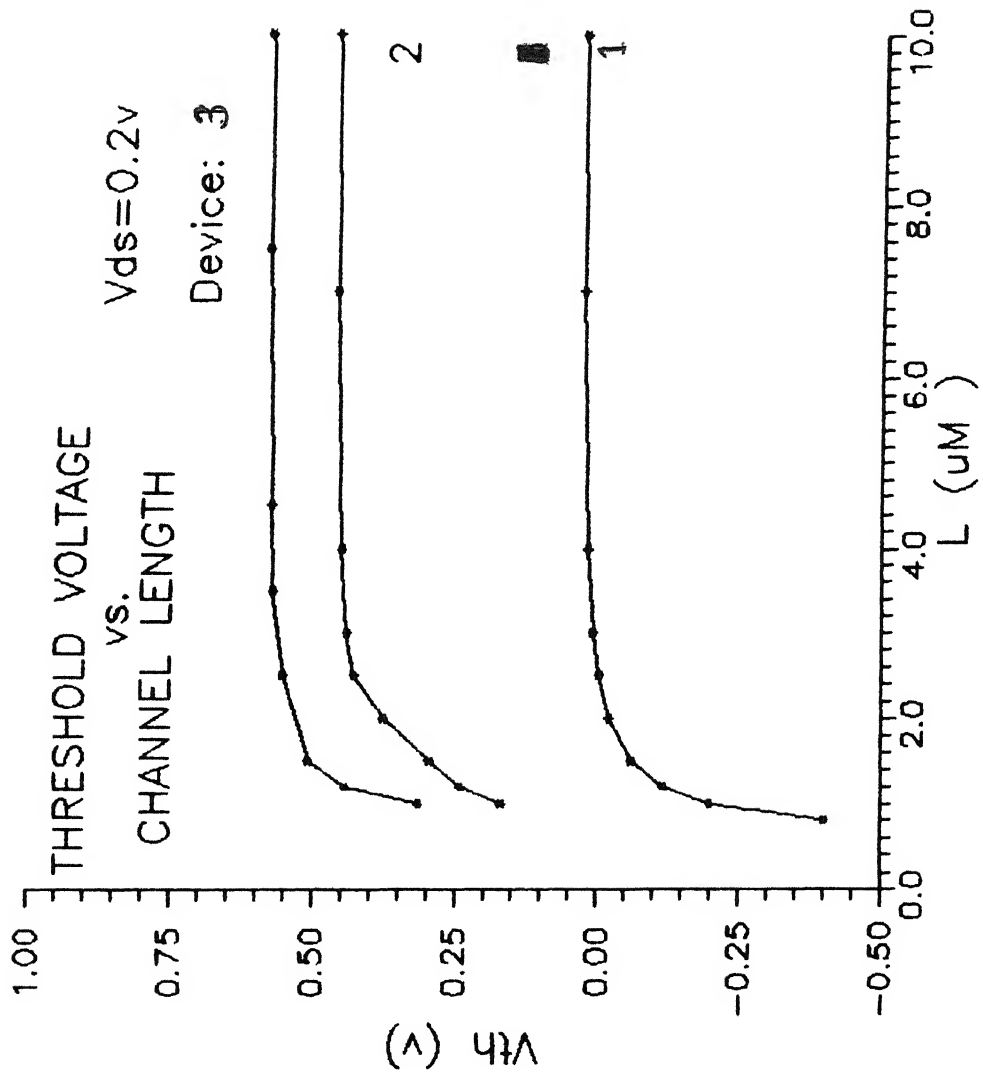


Fig. 6.9
Threshold voltage vs. channel length of the three devices

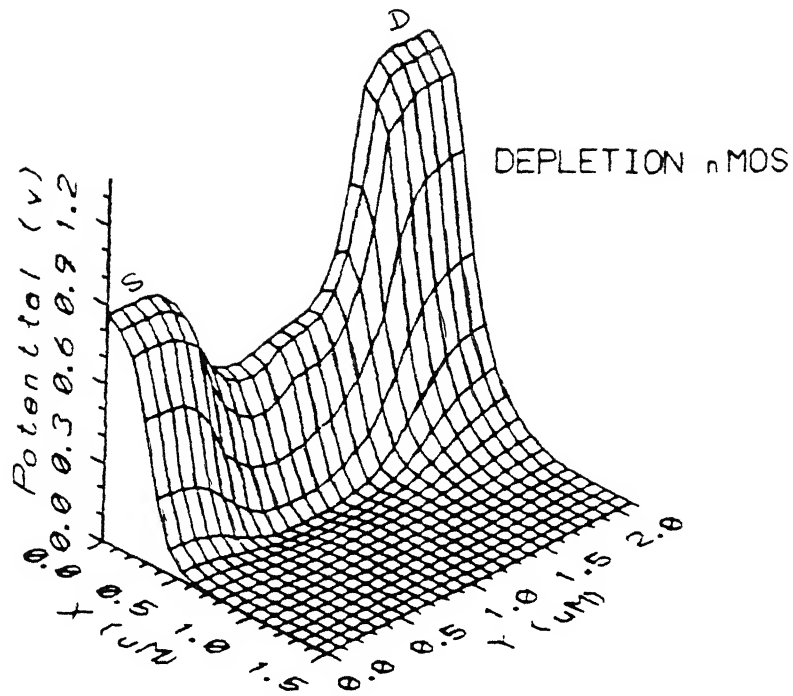


Fig. 6.10a
Potential distribution of the Depletion n-MOSFET
[in depletion mode]

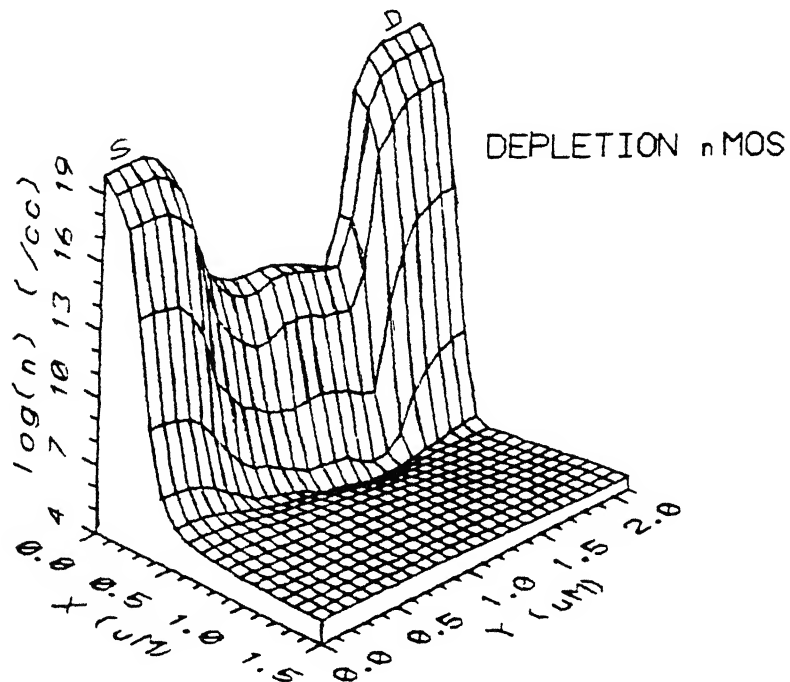


Fig 6.10b
Concentration of electron of the Depletion n-
MOSFET [in depletion mode]

$l=1.5\mu\text{m}$. For DEVICE 2 & DEVICE 3, they are 0.3V & 0.5V respectively. The effect of channel implantations on threshold voltage shift is pretty clear from this plot.

6.3. SIMULATION OF A DEPLETION N-MOSFET :-

A depletion type n-MOSFET of $l=1.5\mu\text{m}$, $w=3\mu\text{m}$, $t_{ox}=500\text{\AA}$; the source-drain and deeper channel implant is similar to that of the DEVICE 3; only the shallow channel implant is changed to donor type (dose = $1 \times 10^{12}/\text{cm}^2$, $r_p=.01\mu\text{m}$ & $drp=.06\mu\text{m}$), and the corresponding flatband voltage is -0.5V.

This device is simulated in the depletion mode, with -1V gate voltage. Quasi three-dimensional plots of potential and electron distribution are shown in fig.6.10a and fig.6.10b respectively.

The output characteristics is shown in fig.6.11 for gate voltage ranging from depletion to enhancement mode operation. The large slope of the characteristics is noticed, as there is no junction in drain & source to channel doping profile and the effect of drain voltage reaches close towards source through this continuous channel.

With the examples presented so far, it is clear that the power of device simulation in understanding the behaviour and in the design of MOSFETs is enormous.

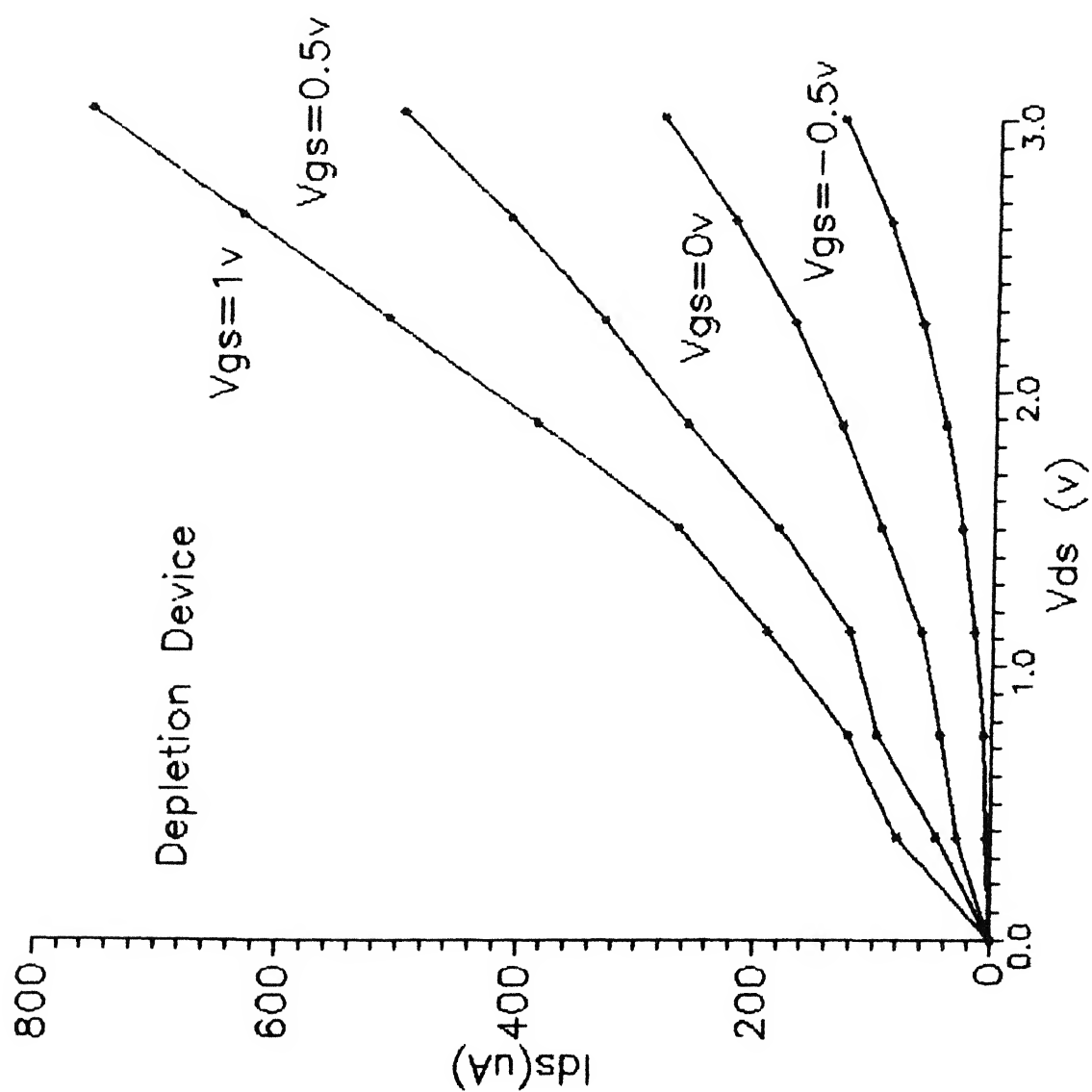


Fig. 6.11
Output characteristics of the Depletion n-MOSFET

Chapter 7

CONCLUSION

A two dimensional numerical model for the MOSFETs has been described and results have been presented as extracted from the program developed for two dimensional planar MOSFET analysis. The results show that the device simulation program can simulate measurable quantities like output characteristics, threshold voltage etc, as well as the quantities which cannot be measured directly, such as potential distribution, carrier concentration distribution etc. within the device. These non-measurable quantities are important to understand the complex behaviour of the integrated device directly, useful in the design process of ICs.

7.1. PROPOSAL FOR FURTHER WORK :-

Now, some scope for the modification and extension of the device simulator developed are outlined below .

7.1a. Modification of this device simulator :

There is, however, a need to develop more accurate model of the physical parameters, of the basic semiconductor equations, specially the doping profile. This may involve complete

re-evaluation of some commonly accepted assumptions and approximations.

In the numerical model (level 2) used here does not include recombination-generation (R). Provision is kept for its inclusion with proper modelling, for the simulation of breakdown behaviour of MOSFETs. In that case both the current continuity equations are to be solved. So computation slows down, hence one can try with other algorithms (like *Newton's method*) to solve the non-linear coupled P.D.Es.

One more modern trend is three dimensional device simulation. As the device dimensions are shrunk, the narrow width effect and effect of the neighbouring devices become predominant. Only the three dimensional simulations can characterize these effects. Then the memory requirement and the computing costs become the major problems; the main routines may be written in the assembly language for faster processing of data as done in case of MINIMOS [13].

7.1b. Integration of process, device & circuit simulators :

In order to make any model predict the performance of the ICs prior to their actual fabrication, it is essential to integrate the process, device and circuit simulators. The device simulator cannot stand alone in the design and development of VLSI. The process parameters (like ion dose, implantation energy, oxidation temperature, etching environments etc.) are set for initial

design. These parameters are fed to the process simulators like *SUPREM* [28], *SUPRA* [29]. They give the doping profile for the device either in one dimension or two dimension. Then this doping profile is fed to the device simulator. The main problems to bridge the device and process simulator are of two types:

(i) If *SUPREM* is used, it gives one dimensional profile, but the device simulators require two dimensional profile. One has to pay attention to the extrapolation of 1-d profile to 2-d [32].

(ii) The second problem is that the mesh of the process simulator is different from that of the device simulator. Error in the interpolation of the impurity concentration on device simulator mesh from the data on the process simulator mesh may cause double junction formation, which creates problem in device simulation [43].

Once these two problems are overcome, the gap between process and device simulator is bridged.

The next is to integrate device and circuit simulations. *SPICE* circuit simulator uses analytical models[44] to describe I-V characteristics. The key to linking technology simulation to circuit is the ability to extract the model parameters from the I-V characteristics obtained by device simulation. This parameter extraction is a separate field. Several parameter extraction algorithms and softwares are developed so far [45]. These parameters are fed to the circuit simulator and small and large signal behaviour, transient response, noise performance etc are simulated.

For a full design of IC, several loops (depends on the complexity of the circuit) are needed from process to circuit simulation and adjustment of the process parameters to achieve the final goal of the circuit .

This type of integration can be done using this device simulator and two other softwares available at IIT, Knapur, *SUPREM* & *SPICE* . Only the bridging softwares are to be developed . Then we will be having a complete CAD tool for VLSI device design.

REFERENCES

1. H.K. Gummel : "A self consistent iterative scheme for one-dimensional steady state transistor calculations", *IEEE tr. on Electron devices*, vol: ED-11, pp:455-465, 1964.
2. A. De Mari : "An accurate numerical steady state one dimensional solution of the p-n junction", *Solid State Electronics*, vol: 11, pp:38-58, 1968.
3. D.L. Scharfetter & H.K. Gummel : "Large signal analysis of silicon read diode oscilltor", *IEEE tr. on Electron Devices*, vol:ED-16, pp:64-67, 1969.
4. D.Vandorpe, J. Borel, G. Merckel, P. Saintot: "An accurate two dimensional analysis the MOS transistor", *Solid State Electronics*, vol:15, pp:547-557, 1972.
5. J.W. Slotboom : "Computer aided two dimensional analysis of bipolar transistors", *IEEE tr. on Electron Devices*, vol:ED-20, pp:669-679, 1973.
6. M.S. Mock : "A two dimensional mathematical model of the insulated gate field effect transistor", *Solid State Electronics*, vol:16, pp:601-609, 1973.
7. T.I. Seidmann & S.C. Choo: "Iterative scheme for computer simulation of semiconductor devices", *Solid State Electronics*, vol:15, pp:1229-1235, 1972.
8. W. Fitchner, D.J. Rose & R.E. Bank : "Semiconductor device simulation", *IEEE tr. on Electron Devices*, vol:ED-30, pp:1018-1030, 1983.

9. R.E. Bank, D.J. Rose & W. Fitchner : "Numerical methods for semiconductor device simulation", *IEEE tr. on Electron Devices*, vol:ED-30, pp:1031-1041, 1983.

10. S.M. Sze : "Physics of semiconductor devices", 2nd. edition, Wiley Eastern, 1986.

11. T. Adachi, A. Yoshii & A. Sudo : "Two dimensional semiconductor analysis using finite element method", *IEEE tr. on Electron Devices*, vol:ED-20, pp:1026-1031, 1979.

12. H.H. Heimler : "A two dimensional analysis of Silicon n-p-n transistor", *IEEE tr. on Electron Devices*, vol:ED-20, pp:708-714, 1973.

13. S. Selberherr, A. Schütz & H.W. Pötzl : "MINIMOS- a two dimensional MOS transistor analyzer", *IEEE tr. on Electron Devices*, vol:ED-27, pp:1540-1549, 1980.

14. T. Toyabe & A. Asai : "Analytical models for threshold voltage and breakdown voltage for short channel MOSFET from two dimensional analysis", *IEEE tr. on Electron Devices*, vol:Ed-26, pp:453-461, 1979.

15. W. Van Roosbroeck : Bell system technical journal, vol-29, pp:560, 1950.

16. B. Meinerzhagen, H.K. Birks, W.L. Engle : "Quasi-simultaneous solution method: A new highly efficient strategy for numerical MOST simulations", *IEEE tr. on Electron Devices*, vol:ED-32, pp:2131-2138, 1985.

17. T. Toyabe : "CADET user's manual", Hitachi central lab.

18. K.M. Cham, S.Y. Oh, D. Chin & J.L. Moll : "Computer aided design and VLSI device development", Kluwer Academic Publishers,

1986.

19. F.H. De la Moneda : "Threshold voltage from numerical solution of the two dimensional MOS transistor", *IEEE tr. on Circuit theory*, vol:CT-20, pp:666-673, 1973.

20. K. Yamaguchi : "Field dependent mobility model for two-dimensional numerical analysis of MOSFETs", *IEEE tr. on Electron Devices*, vol:ED-26, pp:1068-1074, 1979.

21. D.H. Navon & C.T. Wang : "Numerical modeling of power MOSFETs", *Solid State Electronics*, vol:26, pp:287-290, 1982.

22. N.D. Arora & N.D. Hauser : "Electron and hole mobilities in Silicon as a function of concentration and temperature", *IEEE tr. on Electron Devices*, vol:ED-29, pp:292-295, 1982.

23. A.S. Grove : "Physics and technology of semiconductor devices" Wiley, New York, 1967.

24. K.K. Thornber : "Relation of drift velocity to low field mobility and high field velocity saturation", *Jl. of Applied Physics*, vol:51, pp:2127-2136, 1980.

25. S. Selberherr : "Analysis and simulation semiconductor devices", Springer Verlag, 1984.

26. F.F. Fang & A.B. Fowler : "Transport properties of electron in the inverted surface", *Physical Rev.*, vol:169, pp:619-631, 1968.

27. W.L. Engle, H.K. Dirks & H.K. Meinerzhagen : "Device modelling", *Proc. IEEE* -71, pp:10-33, 1983.

28. D.A. Antoniadis : "One-dimensional simulation of IC fabrication process", in: *Process and Device simulation for*

MOS-VLSI circuits, NATO ASI Series, Martinus Nijhoff, pp:226-263, 1983.

29. M. Kump & R.W. dutton : "Two-dimensional process simulation", in: *Process and Device simulation for MOS-VLSI circuits*, NATO ASI Series, Martinus Nijhoff, pp:304-342, 1983.

30. A.R. Mitchell & F.D. Griffiths : "The finite difference method in partial differential equations", John Wiley , 1980.

31. G.E. Forsyth & W.R. Wasow : "Finite difference methods for partial differential equations", Wiley, 1960.

32. S. Selberherr, A. Schütz & A.H. Pötzl: " Two dimensional MOS transistor modelling", in: *Process and Device simulation for MOS-VLSI circuits*, NATO ASI Series, Martinus Nijhoff, pp:304-342, 1983.

33. J.F. Hart, E.W. Cheney, C.L. Lawson & H.. Maehly: "Computer approximations", Wiley, New York, 1968.

34. M.S. Mock : "An initial value problem from semiconductor device theory." *SIAM Jl. of Mathematical Analysis*, vol:5, pp:597-612, 1974.

35. M.S. Mock : "On convergence of Gummel's numerical algorithm", *Solid State Electronics*, vol:15, pp:1-4, 1972.

36. H.L. Stone : "Iterative solution of implicit approximations of multidimensional partial differential equations", *SIAM Jl. of Numerical Analysis*, vol:5, pp:530-558, 1968.

37. R.S. Varga : "Matrix iterative analysis", *Pretice Hall, Inc.*, 1962.

38. J.A. Greenfield and R.W. Dutton : "Non-planar VLSI analysis using Poisson's equation", *IEEE tr. on Electron Devices*, vol:ED-27, pp:1520-1532, 1980.
39. K.A. Salsburg, P.E. Cottrell & E.M. Buturla : "FIELDAY-finite element device analysis", in: *Process and Device simulation for MOS-VLSI circuits*, NATO ASI Series, Martinus Nijhoff, pp:582-619, 1983.
40. H.C. Pao & C.T. Sah : "Effect of diffusion current on characteristics of Metal-Oxide(insulator)-Semiconductor transistors", *IEEE tr. on Electron Devices*, vol:ED- 9, pp:927-937, 1966.
41. H.G. Lee, S.Y. Oh, G. Fuller : "A simple and accurate method to measure threshold voltage of an enhancement mode MOSFET", *IEEE tr. on Electron Devices*, vol:ED-29, pp:346-348, 1982.
42. J.A. Greenfield , R.W. Dutton & Price : "Analysis of non - planar devices", In: *Process and Device simulation for MOS- VLSI circuits*, NATO ASI Series , Martinus Nijhoff, pp:432-489, 1985.
43. R.J. Sokel, B. Donald, B. Macmillan : "Practical integration of process device and circuit simulation ", *IEEE tr. on Electron Devices*, vol:ED-32, pp:2110-2116, 1985.
44. A. Vladimirescu, K.Zhang, A.R. Newton et al: "SPICE version 2G users guide", Dept. of Electrical Engg & Computer Sc., University of California, Berkeley, 1981.
45. P. Yang & P.K. Chatterjee : "An optimised parameter extraction model program for MOSFET models", *IEEE tr. on Electron Devices*, vol:ED-30, pp:1224-1219, 1983.

TITLE & END :

DEVICE, PROFILE, BIAS, OPTION & COMNT

The individual indents and the keys under them are described below.

(i) **DEVICE** : It describes the channel type and the geometry of the planar MOSFET. The keys under this are:

TYPE : for nMOS (pMOS) it is equated to 'n' ('p').

L : gate mask length, **W** : channel width, **TOX** : oxide thickness, **SD** : source & drain contact lengths, **D** : simulation depth. They all are real numbers in cm units (need not be specified). All the keys are to be defined.

(ii) **PROFILE** : It describes the doping profile of MOSFET, from the parameters given here the program generates a 2d doping profile. The keys under this indent are :

SUBS : substrate doping concentration (in /cc), if the impurity is p-type then the real value assigned to it must be negative (as ionized accepters are negatively charged), for donor type it is positive.

DOSE : source & drain implant dose (in atoms/cm²), for accept or type value must be negative and vice versa.

RP : range of source & drain implantation, **DRP** : straggle for the same. They are real numbers in cms.

DOSEC1 : dose for 1st channel implantation (unit and sign convention is as DOSE), **RPC1** & **DRPC1** : are the range and straggle (in cm) for 1st. channel implantation.

DOSEC2, RPC2 & DRPC2 : are the corresponding quantities for 2nd. channel implantation. Any one or both of the sets (DOSEC1, RPC1, DRPC1) and/or (DOSEC2, RPC2, DRPC2) may be omitted, then it is assumed that the corresponding channel implantation is not done. But the other four PROFILE keys must be defined .

(iii) BIAS : It describes the terminal biases and interface quality. The keys are :

US, UG, UD & UB : are source, gate, drain and bulk voltages in volts respectively.

PHIMS : gate metal-semiconductor work function difference in volts, QINT : interface trapped charge density (in coulomb/cm²), VFB : flat band voltage in volts.

The value assignment to these keys are optional and if not specified default values are 0. If PHIMS & QINT are specified, no need to specify VFB. If VFB is specified, it overrides PHIMS & QINT.

(iv) OPTION : It describes what type of simulation the user wants and the parameters related to these simulations. The keys are :

MODEL : it is equated to a particular option of simulation supported by the program. The options supported are as follows -

'DISTRIB' - gives distribution of potential, carriers & doping concentrations at grid points in the output file.

'IVCHAR' - gives the output characteristics (I_{ds} vs V_{ds} for

different V_{gs}), two parameters are to be defined along with this model. They are **NGSTEP** & **NDSTEP**, equated to the integers i.e., the number of gate voltage steps and drain voltage steps for output characteristics. The values assigned to **UG** & **UD** in the **BIAS** card become the final values for the output characteristics calculation. If **NGSTEP** & **NDSTEP** not specified, default is taken to be (1,1).

'**VTHRES**' - it calculates threshold voltage. **UD** of **BIAS** card must be a non-zero quantity and **UG** defines the initial guess for threshold voltage using the scheme described in sec.5.3b.

'**SUBTHRES**' - gives subthreshold characteristics. **NGSTEP** must be specified in this card, defines the number of points to be calculated upto the gate voltage specified by **UG** of **BIAS** card, and **UD** must be non-zero quantity.

These model names must be quoted inside single inverted commas, written either in lower case or upper case letters, mixing of case is not allowed.

T : this key is optional for specifying absolute temperature in $^{\circ}\text{K}$, default value is 300°K .

(c) **COMNT** : the card under this indent contains comment, if the user wants to give any, this is ignored by the program.

Important points to note :

1) When a line becomes too long the user may break the line into several lines and the continuation lines must start with a

plus sign (+) within first 10 columns of a line.

2) Except TITLE & END cards, other cards may be shuffled.

3) All the lengths are in cms, concentration in /cc, biases are in volts, temperature in °K, doses in atoms/cm² etc. as described above. One should not specify the units in the input file.

4) All values are real numbers (written in F or E format) except NGSTEP & NDSTEP, they are integers. Character strings equated to TYPE & MODEL are quoted inside '...' .

Examples of the input files are shown in the figure 6.1. of chapter 6.

ABSTRACT

Name: TAPAS NANDI

Roll No.: 8810456

Degree for which submitted: M.Tech.

Department: ELECTRICAL ENGINEERING

Institute: INDIAN INSTITUTE OF TECHNOLOGY, KANPUR.

Title of the thesis: A TWO DIMENSIONAL SIMULATION OF MOSFETS

Thesis supervisor: Dr. M.M. HASAN

Month & year of submission: MARCH, 1990

The most effective way to design VLSI MOSFET structures is to use a sophisticated complex two dimensional model. Such a model, using the basic semiconductor equations along with the accurate models for the physical parameters of the basic equations, has been described here. Numerical simulation of this MOSFET model using finite difference method has also been described. Low computation cost algorithms have been used to develop an easy-to-use software package for planar MOSFET simulation. Simulated results are presented for few types of short channel MOSFETs to show the power of the device simulation to predict the behaviour of the device. Finally, the modifications of this MOSFET simulation model and the possibility to integrate this device simulation with the process and the circuit simulations have been proposed.

